DEVELOPMENT AND ANALYSIS OF A NEW DGPS ATTITUDE DETERMINATION METHOD FOR MINIATURE SATELLITES

STEFANO TORRESAN

Dipartimento di Ingegneria Industriale
Corso di Laurea Magistrale in Ingegneria Aerospaziale
Universitá degli Studi di Padova

Relatore: Ing. Alessandro Francesconi
Co-relatore: Ing. Lorenzo Olivieri

ABSTRACT

In this thesis the concept of attitude determination with phase carrier differential GPS measures for miniature satellites is analysed, with particular attention dedicated to the effects of the short antenna baseline. At first the main features of the GPS and the GPS signal are outlined. The problem of attitude determination is presented, with particular focus on the QUEST algorithm. The concept of phase carrier DGPS measure is introduced along with the main DGPS-related experiments, such as RADCAL and TOPSAT; the algorithm required to convert the phase difference measure into a vectorized measure is also derived. Two antenna layouts based on a Cubesat standard miniature satellite are proposed, with four patch and four helix antennas respectively, and their merits are evaluated through a number of simulations aimed to analyse the satellite availability and the attitude estimation accuracy for each one. Finally the patch antenna layout is identified as the most promising design and its performances compared with the current attitude determination and control systems available off-the-shelf for the Cubesat platform.

SOMMARIO

In questa tesi viene analizzata l'idea di un sistema di determinazione d'assetto basato su misure differenziali di fase della portante del segnale GPS, con una particolare attenzione rivolta agli effetti della distanza ridotta tra le antenne. Vengono inizialmente introdotte le caratteristiche fondamentali del sistema GPS e del segnale GPS. Il problema della determinazione d'assetto viene presentato, con particolare attenzione rivolta all'algoritmo QUEST. Il concetto base delle misure differenziali di fase viene poi introdotto assieme ai principali esperimenti ad esso collegati, come RADCAL e TOPSAT; in seguito vengono derivati gli algoritmi necessari per convertire le misure di fase in vettori. Vengono proposti due schemi con rispettivamente quattro antenne a mictrostriscia e quattro antenne ad elica, le loro caratteristiche vengono comparate attraverso diverse simulazioni volte ad analizzare la disponibilitá dei satelliti GPS e le loro performance in termini di accuratezza nella stima dássetto. Lo schema piú promettente risulta essere quello con le antenne a microstriscia, le cui caratteristiche vengono comparate con i sistemi di determinazione e controllo d'assetto per Cubesat disponibili sul mercato.

CONTENTS

1 INTRODUCTION 1
- 1.1 Attitude determination 1
- 1.2 Differential GPS 3
- 1.3 Miniaturized satellites 4
- 1.4 Motivation 5
  - 1.4.1 Content summary 6

2 GPS OVERVIEW 9
- 2.1 GNSS 9
- 2.2 Overview of the GPS architecture 10
- 2.3 Trilateration 10
- 2.4 GPS signal characteristics 12
  - 2.4.1 Pseudo-Random Noise modulations 12
  - 2.4.2 Navigation Message 12
  - 2.4.3 C/A Signal generation 13
- 2.5 GPS receiver 13
  - 2.5.1 Antenna 13
  - 2.5.2 RF frontend 15
  - 2.5.3 Downconversion 16
  - 2.5.4 Digitalization 16
  - 2.5.5 Baseband signal processing 16

3 CARRIER PHASE DIFFERENTIAL GPS 17
- 3.1 Attitude parametrization 17
  - 3.1.1 Reference frames 17
  - 3.1.2 Parametrization of rotation 18
- 3.2 Original attitude determination problem 19
  - 3.2.1 Quaternion parametrization 23
  - 3.2.2 Eigenvalues estimation 25
- 3.3 DGPS concept 29
- 3.4 GPS attitude determination 31
  - 3.4.1 Sightlines in body frame 32
  - 3.4.2 Baselines in reference frame 32

4 SIGNAL AVAILABILITY 35
- 4.1 Simulation parameters 35
  - 4.1.1 Orbit geometry 35
  - 4.1.2 GPS antenna 37
  - 4.1.3 Receiving antenna 37
- 4.2 Simulation results 41
  - 4.2.1 General considerations 41
  - 4.2.2 Patch 42
  - 4.2.3 Helix 42

5 ATTITUDE ESTIMATION ACCURACY 49
- 5.1 Error sources 49

5.1.1 Propagation 50
5.1.2 Multipath 50
5.1.3 Carrier to noise ratio 51
5.1.4 Antenna phase center 51
5.1.5 Receiver specific error 52
5.2 Simulations 54
5.2.1 Simulation procedure 54
5.2.2 Simulation results 55
6 CONCLUSIONS 63
6.1 Design evaluation 63
6.2 Comparison with available miniature satellite ADCS 64
6.3 Future work 65
6.3.1 In-depth receiver simulation 65
6.3.2 Kalman filtering 65
6.3.3 Experimental test 65
BIBLIOGRAPHY 67

LIST OF FIGURES

Figure 1 The Differential GPS concept 3
Figure 2 nCube2, a one unit Norwegian built Cubesat 5
Figure 3 Structure of the thesis, chapters are color-coded 7
Figure 4 Intersection points of three spheres 11
Figure 5 Modulation of the L1 signal 13
Figure 6 Structure of the L1 signal 14
Figure 7 GPS receiver diagram 14
Figure 8 Typical patch antenna gain pattern 15
Figure 9 Effect of signal reflection on a Right Handed Circular Polarized antenna, the reflected signal is not received. 15
Figure 10 Choke ring around a GPS antenna, mitigating multipath effects (source: Trimble website). 16
Figure 11 RPY coordinates 17
Figure 12 Body coordinates 18
Figure 13 Speed comparison[1] for robust estimation (q-method and SVD, top figure) and fast estimation algorithms (QUEST and ESOQ, bottom figure) 22
Figure 14 QUEST algorithm block diagram 28
Figure 15 The phase difference of the signal received from two antennas 29
Figure 16 Concept scheme of two antennas DGPS 30
Figure 17 Integer ambiguity 30
Figure 18 Examples of antenna geometry: on the left they are arranged in a coplanar fashion, non compatible with equation 42 32
Figure 19 GPS satellites position relative to the GPS YUMA almanac, week 761 36
Figure 20 Polar diagram of a generic radiation pattern 38
Figure 21 GPS signal main lobe 38
Figure 22 Patch and helix antennas, the patch antenna is 25x25x4.5 mm 39
Figure 23 The two proposed layouts 39
Figure 24 Patch antenna beamwitdh 40
Figure 25 Helix antenna beamwitdh 41
Figure 26 Satellite visibility history, patch antenna, bw=120°, alt=300km 43
Figure 27 Number of visible satellites, patch antenna, bw=120°, alt=300km, i=0° 44

Figure 28 Cumulative number of visible satellites with different inclinations, patch antenna, bw=160°, alt=300km 45
Figure 29 Cumulative number of visible satellites, patch antenna, bw=90°, i=0° 45
Figure 30 Cumulative number of visible satellites, patch antenna, bw=120°, i=0° 46
Figure 31 Cumulative number of visible satellites, patch antenna, bw=160°, i=0° 46
Figure 32 Cumulative number of visible satellites, helix antenna, bw=180°, i=0° 47
Figure 33 Cumulative number of visible satellites, helix antenna, bw=260°, i=0° 47
Figure 34 Effect of baseline length on baseline vector estimation in presence of errors 50
Figure 35 Effect of antenna phase center uncertainty on baseline definition 51
Figure 36 Block diagram of attitude estimation simulations 53
Figure 37 Influence of sightline geometry on attitude accuracy 56
Figure 38 Attitude estimation accuracy, patch antenna, bw=120°, h=300km, noise=2.5mm. The dotted lines are the 3σ bound for attitude error 57
Figure 39 Attitude estimation accuracy, patch antenna, bw=160°, h=300km, noise=2.5mm. The dotted lines are the 3σ bound for attitude error 58
Figure 40 Average 3σ attitude error, patch antenna, bw=120° 59
Figure 41 Average 3σ attitude error, patch antenna, bw=160° 60
Figure 42 Average 3σ attitude error, helix antenna, bw=260° 61

LIST OF TABLES

Table 1 Attitude determination sources comparison 2
Table 2 RMS attitude error for the RADCAL experiment 4
Table 3 Representation of attitude 20
Table 4 The YUMA entry for satellite 01, week number 761 (October 2013) 36
Table 5 Average availability time, patch antenna 44
Table 6 Average availability time, helix antenna 44
Table 7 Modeled error sources and average values 52

Table 8 Comparison of 3σ attitude errors for RADCAL, TOPSAT and the proposed DGPS sensor 64

1 INTRODUCTION

1.1 ATTITUDE DETERMINATION

Attitude determination is the process of *estimating the orientation of an object in space*, using informations provided by dedicated instruments. Attitude is expressed by the rotation of a *body frame* (axis fixed to the object) with respect to a predefined *reference frame*. Attitude knowledge is required throughout all the spacecraft's mission profiles, in operations such as main engine burn, proper payload orientation (like telecommunication antennas or telescopes) and many housekeeping functions (radiator and solar panel orientation).

To obtain such information many different sensors exist, each one using different reference objects (sun, earth or star trackers and magnetic field sensors) or exploiting different physics principles (inertial measurement units). Sensors that use external reference (all but IMUs) provide the versor of the reference entity in body frame, by knowing the same versor in relative frame it is possible to estimate the rotation of the body frame w.r.t. the reference frame. IMUs usually provide angular rates that are used to estimate the attitude between the instants of acquisition of the other sensors, called "fixes", if required.

An attitude determination system is usually composed by many types of these sensors, to provide redundancy and to complement each other's pros and cons (summed up in table 1, adapted from Wertz's *Spacecraft Attitude Determination and Control* [2, p. 17]). IMUs are always used because no other sensor has the same peculiar characteristics, i.e. continuous measurements and no external sensors; while the rest of the attitude determination system is a mix of other sensors that depend on required performance, resources budget and orbit characteristics.

After the measurements have been taken, an algorithm has to estimate the attitude given the reference versors in body frame and reference frame; the former provided by sensors and the latter reconstructed from the orbital position of the spacecraft and the observed sources. This process is carried out on by onboard computers.

Table 1: Attitude determination sources comparison

Reference	Advantages	Disadvantages
Sun	Bright, unambiguous, low power and weight. Usually must be known for solar cells and equipment protection	Subject to eclipses from central body; 0.5 deg angular diameter viewed from Earth limits accuracy to 1 arc minute
Earth	Always available for nearby spacecraft, bright; largely unambiguous (may be Moon interference); necessary for many types of sensor and antenna coverage	Sensors must be protected from Sun, resolution limited to 0.1 deg because of horizon definition, orbit and attitude strongly coupled
Magnetic field	Economical, low power requirements, always available for low altitude spacecraft	Poor resolution ($>$ 0.5 deg), good only near Earth, limited by field strength and modeling accuracy, orbit and attitude strongly coupled, spacecraft must be magnetically clean (or inflight calibration is required), sensitive to biases
Stars	High accuracy (10^{-3} deg), available anywhere in the sky, essentially orbit independent except for velocity aberration	Sensors heavy, complex and expensive. Identification of stars for multiple target sensors is complex and time consuming, usually require second attitude system for initial attitude estimates
Inertial	Requires no external sensors, orbit independent, high accuracy for limited time intervals, easily done onboard	Senses angular velocities, subject to drift, sensors may have rapidly moving part subject to wear and friction, relatively high power and large mass

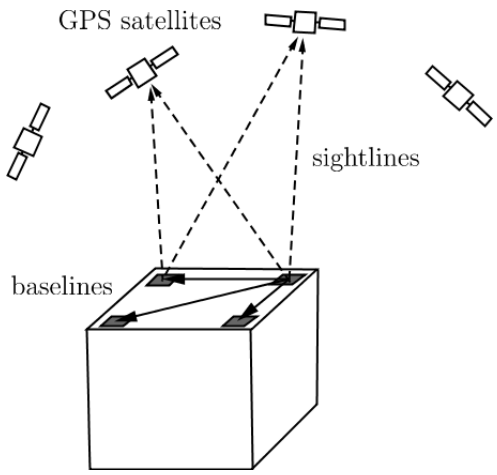

Figure 1: The Differential GPS concept

1.2 DIFFERENTIAL GPS

The Global Positioning System network, fully operative since the early nineties, grants global positioning service not only to ground users but also to spacecraft; the number of visible GPS satellites is reduced as the altitude increases.

While orbit determination is the most obvious application of space-based GPS, attitude determination is also possible[3]. Using multiple antennas and analysing the carrier phase of the signal received from multiple satellites it is possible to estimate the line of sight vector between the spacecraft and each visible GPS satellite (sightline), then the orientation of the vector connecting two antennas (called baseline) can be reconstructed; using at least three baselines the attitude of the platform can be estimated. This is shown in figure 1.

A differential-GPS attitude sensor offers many advantages:

- unique platform for orbit position and attitude determination
- precise timing available as a free by-product of the measure
- small impact on resources (mass, volume and power)
- independent from time and orbit position
- external reference measure (unlike IMUs) with a high rate (up to 1 Hz and more)

DGPS attitude sensors have been proposed since the eighties and some spacecraft used this technology, such as RADCAL[3][4] and GADAC[5] in the early nineties, while TOPSAT[6] and Minnesat[7] are more recent and miniaturized experiments.

RADCAL (RADar CALibration) is a gravity gradient stabilized small satellite launched in 1993 that was used to calibrate several radar system of the United State Department of Defence (DoD), it carried four GPS antennas, with baselines around 60cm or less, and two GPS receivers in order to test the concept of DGPS attitude determination.

The data acquired throughout the mission were used to develop and test the first algorithms for integer ambiguity resolution but were not used or processed on-board. The attitude accuracy range was initially around 1° (1σ) but more accurate estimates were developed, the result is reported in table 2 (adapted from [4, p. 78])

Table 2: RMS attitude error for the RADCAL experiment

Component	Min RMS error [deg]	Max RMS error [deg]	Average RMS error [deg]
Yaw	0.271	0.415	0.317
Pitch	0.457	0.533	0.495
Roll	0.457	0.536	0.496

TOPSAT (Tactical OPerational SATellite) is a micro-satellite demonstrator with a high resolution telescope developed by Surrey Satellite Technology and launched in 2005. As a secondary attitude determination system it carries four GPS patch antennas with a baseline of 0.6m, the spacecraft performed several experiment both in a nadir-pointing attitude and in a pitch/roll off-boresight mode, the attitude estimation was performed on-board with a 1Hz update rate.

The results for this experiments in terms of attitude estimation disparity (between the primary ADCS[1] and the DGPS) where 0.61° RMS in roll, 0.71° RMS in pitch and 1.29° RMS in yaw; however the DGPS measure for the yaw angle was considered more accurate than the ADCS one leading to a estimated yaw error of 0.5° RMS.

1.3 MINIATURIZED SATELLITES

Miniaturized satellites, with the notable example of Cubesats, grant access to the design and construction of operative spacecraft to Universities (such as the nCube2, figure 2 (source: Wikipedia)), small companies and even private users.

Cubesats are composed of one or several units, each one is 10cm x 10cm x 10cm; their small dimensions impose severe constraints to the resource budget allowed to attitude determination, nonetheless

1 Attitude Determination and Control System

Figure 2: nCube2, a one unit Norwegian built Cubesat

many miniaturized attitude sensors exist.

Miniature satellites have been used to perform Earth remote sensing, tethered spacecraft tests, spacecraft subsystem tests and for educational purposes.

While standard GPS receivers have been developed for miniature satellites application, currently no DGPS attitude sensor exist.

1.4 MOTIVATION

The purpose of this thesis is to evaluate the performance of a DGPS attitude sensor for miniature satellite applications, identifying the main sources of error and analysing their influence on the attitude estimate.

While the DGPS technology is being researched for more than twenty years, it was limited to isolated experiment.

The advantages presented by this technology suit perfectly a miniaturized application such as Cubesats and the related constraints, however this approach has not been followed before because of the drastic reduction of antenna baseline: while previous DGPS experiments had baselines around 0.6m, a DGPS sensor in a Cubesat is limited to 0.1m; this can reduce considerably the accuracy of the attitude estimation.

In order to evaluate the performances of such miniaturized system it is necessary to analyse both its hardware and software elements and to model the errors that perturb the attitude estimate; these errors are modeled in terms of phase noise, the main DGPS measurement.

While it is found that the state of the art technologies are not suited for this application, because the performance that they provide are

not enough for an accurate error estimate, it is possible to formulate the requirements for the next generation receiver and also identify an optimal antenna layout.

1.4.1 *Content summary*

Chapters 2 and 3 are devoted to an introduction to GPS, attitude determination and differential GPS concept; the algorithms for attitude determination with differential GPS phase measures also will be presented in depth.

The simulations address two issues: availability of GPS satellite in low earth orbit and accuracy of the DGPS attitude estimation: this will be the subjects of the following two chapters, each one will begin with the description of the models and configurations utilized, followed by the analysis of the results. The final chapter will outline the main results as well as provide a comparison of the DGPS sensor with the current state of the art Cubesat sensors. The overall thesis structure is outlined in figure **??**.

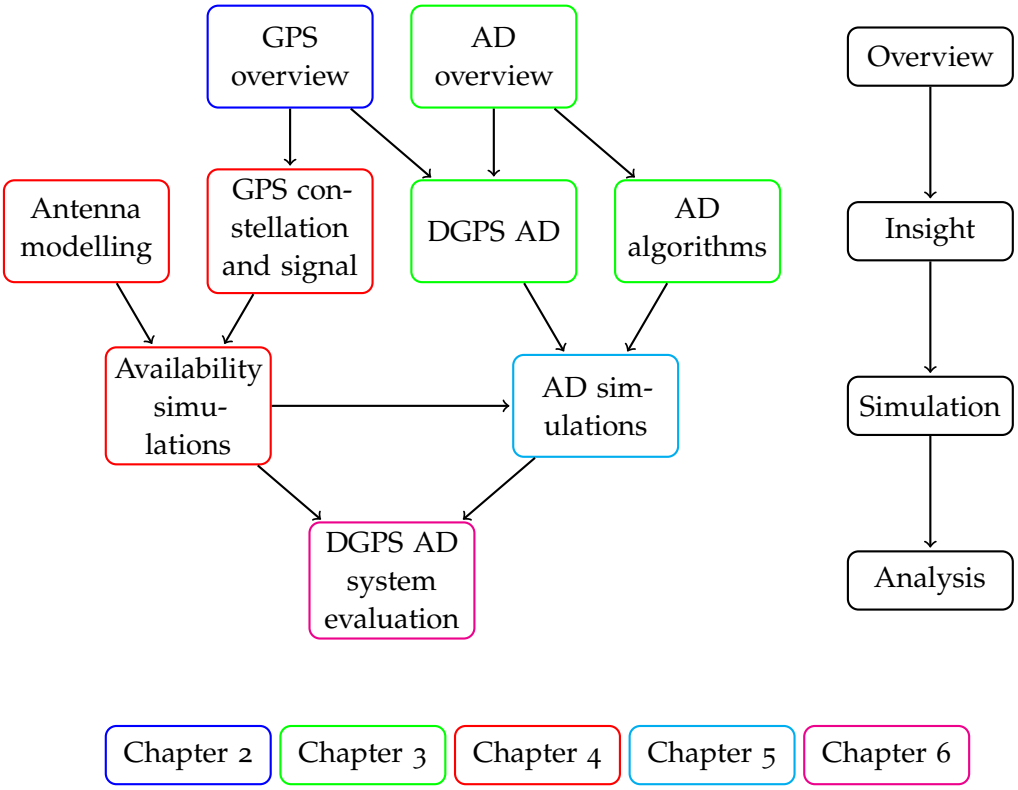

Figure 3: Structure of the thesis, chapters are color-coded

2 GPS OVERVIEW

SUMMARY

This chapter will present an introduction to the Global Navigation System. At first the different GNSS available or proposed are reviewed, then a more GPS-focused section will follow with an overview on the GPS architecture.

The concept of trilateration, as well as the bases of GPS signal characteristics and a scheme of a GPS receiver, are introduced to give a basic understanding on the GPS function.

The main reference sources used throughout this chapter are *Global Positioning System Theory and Applications* [8] and *Global Positioning Systems, Inertial Navigation, and Integration*[9].

2.1 GNSS

A Global Navigation Satellite System (GNSS) is a combination of satellite constellation and ground infrastructure that provides accurate positioning with a global coverage. There are several GNSS systems both operational and under development:

- GPS (Global Positioning System): the first GNSS, developed by the USA for military and civilian use. It uses a semi-synchronous Medium Earth Orbit (MEO) constellation with 32 satellites.
- GLONASS (GLObal NAvigation Satellite System): the Russian equivalent to the GPS, it suffered from incomplete coverage until the 2000s. 24 satellites are used in this system.
- Galileo: the European civil-oriented GNSS, currently under deployment with four satellites in orbit; to be completed by 2019 (30 satellites constellation).
- BeiDou-2: the upgrade of the Chinese BeiDou-1, composed by satellites in different orbits (3 geosynchronous[1], 5 geostationary[2] and 27 Medium Earth Orbit) and to be completed by 2020.

Other positioning systems have similar concept but offer a limited coverage:

1 The geosynchronous orbit, or GSO, is a circular orbit with a period of exactly one sidereal day (23h 56m 4s), this is achieved at an altitude of 35,786km.

2 The geostationary orbit, or GEO, is a particular geosynchronous orbit with no inclination: this allows the relative position of the spacecraft and an Earth observer to be constant (the spacecraft seems still in the sky).

- IRNASS (Indian Regional Navigation Satellite System): under development, the proposed system uses 7 satellites in both geostationary and geosynchronous orbit.
- BeiDou-1: it is owned by China and currently offers a regional coverage.

While different in some aspects, most of these systems share many similarities. Because of its importance and widespread use the GPS will be analysed further in detail, but the same goes for the majority of the GNSS systems worldwide.

2.2 OVERVIEW OF THE GPS ARCHITECTURE

The Global Positioning System is composed by:

- the *Space Segment*: 32 satellites arranged in six orbital planes, four satellites for each plane, with an orbital inclination $i = 55\,\text{deg}$; the planes are evenly spaced with a RAAN (Right Ascension of the Ascending Node) separation of $\Omega = 60\,\text{deg}$. The orbits radius is approximately 26.600km (altitude of 20.200km) in order to have an orbital period of half a sidereal day ($11\text{h}\,58\text{m}\,2\text{s}$), this grants that every satellite repeats the same groundtrack twice a day and at least six satellites are always in view from any point on the surface of the Earth.
- the *Control Segment*: composed by a number of ground station (1 master, 1 alternate master, 4 ground antennas and 6 monitor stations) spread all over the world; they are operated by the US Air Force and continuously monitor the GPS constellation, track the position of each satellite and update the ephemeris for the navigation message.
- the *User Segment*: any military, civil or commercial GPS receiver.

The GPS reached initial operational capability in 1993 with 24 satellites in orbit transmitting the Standard Positioning Service (SPS), in 1995 achieved the full operational capability with the Precise Positioning Service (PPS, available only to military users). By 2000 the civil signal is no longer disturbed, the so-called Selective Availability (SA), granting an accuracy better than 20 meters; future GPS satellites won't be able to perform SA.

2.3 TRILATERATION

A GPS receiver measures the time of flight of a signal transmitted from an orbiting satellite to a receiver, in this signal are coded the information regarding satellite time and position at the instant of transmission. Since the signal moves at the speed of light it is possible to

measure the distance from the satellite to the receiver by knowing the sending and receiving time. The locus of points with the same distance from a reference point is a sphere.

The trilateration is the process of determining the position of a point in space by measuring the distance from reference points of known position. In three-dimensional geometry the intersection of three non-collinear spheres is composed of two points: at least three reference points are therefore needed to compute the position of the unknown point, narrowing it down to two points. This is shown in figure 4.

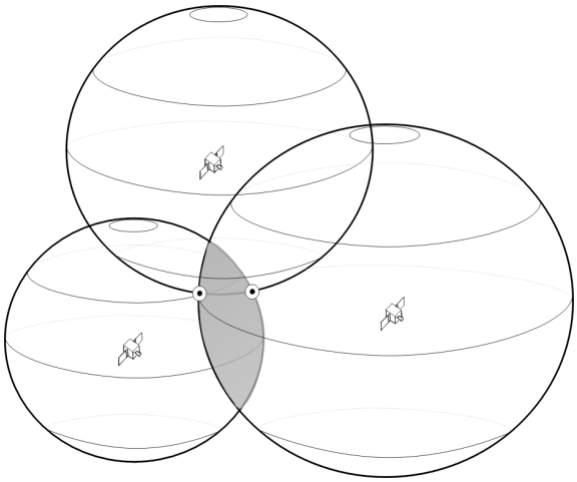

Figure 4: Intersection points of three spheres

Translating this concept to GPS gives the minimum information that the receiver requires in order to determine its own position:

- Satellite position at the instant of transmission
- Satellite time at the instant of transmission
- Receiver time at the instant of reception

The main source of error in this procedure is the time: at the speed of light an error of $1\mu s$ in the time of flight measure becomes a $300m$ error in range. This is why ultra-stable atomic clocks are used on board the satellites, granting a time accuracy of $\pm 10ns$.

However it is not possible to build a small-sized commercial receiver with the same time accuracy, so the synchronization error between the satellite clock and the receiver clock is included in the position determination algorithm, raising to four the minimum number of satellites required to obtain a position fix; this is a fundamental concept in GPS navigation.

The concept behind any GNSS is code ranging, a technique to obtain a position fix from a number of coded signals.

In the case of the GPS the signal is composed by a high-frequency *carrier*, a low-frequency *Pseudo-Random Noise* (PRN) modulation and a even lower-frequency *Navigation Message* (NM) modulation. While the carrier frequency is single, PRN and NM are unique to each satellite, enabling the receiver to acquire and discriminate different signals transmitted on the same carrier. Both PRN and NM are binary modulations. For the GPS the carrier frequencies are ($f_0 = 10.23MHz$):

- L1: $f_{L1} = 154 f_0 = 1575.42MHz$
- L2: $f_{L2} = 120 f_0 = 1227.60MHz$

2.4.1 *Pseudo-Random Noise modulations*

The purpose of a PRN code is both to identify the satellite and to provide a sequence to which the receiver can "lock", isolating the message sent from one satellite from the others. There are different Pseudo-Random Noise modulations, both on L1 and L2:

- The Coarse Acquisition (C/A) code modulates L1 and is composed by 1023 impulses at a frequency of $0.1 f_0 = 1.023MHz$, the signal repeats itself every $1ms$. This signal is public, meaning that the PRN codes are stored inside the GPS receiver in order to make it capable to acquire the signal.
- L2C is similar to C/A, it modulates L2 with 10230 impulses at a frequency of $0.1 f_0 = 1.023MHz$ the signal repeats itself every $01ms$. This signal is public and transmitted from Block IIR-M satellites and later.
- P(Y) is the encrypted military code on L2, is composed by a very large number of impulses and it repeats itself every 37 weeks
- M is a new military code that modulates both L1 and L2, no information on this code is available.

2.4.2 *Navigation Message*

The Navigation Message contains informations about the satellite date and time, health, ephemeris and the almanac (status, position and PRN number of all GPS satellites). Its frequency is 50Hz and the signal is composed by 25 blocks 30 seconds each, for a total 12.5 minutes of duration of the transmission.

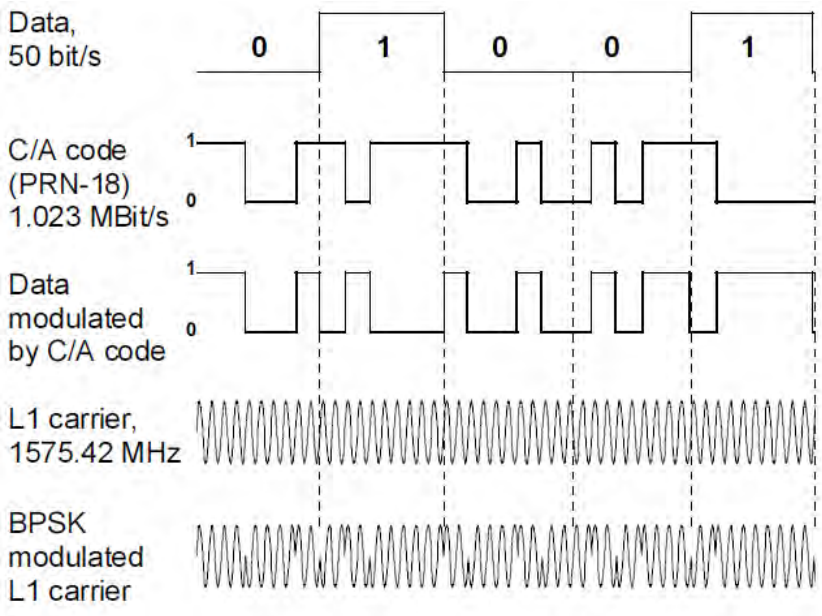

Figure 5: Modulation of the L1 signal

2.4.3 *C/A Signal generation*

It is shown in figures 5 and 6 (source: *Global Positioning Systems Inertial Navigation and Integration*[9]) the structure of the L1 carrier modulated with the C/A code and the Navigation Message.

2.5 GPS RECEIVER

In order to access the information transmitted the encoded GPS signal must be received and acquired properly. The GPS receiver is composed by the following elements, that process the signal in cascade:

- Antenna
- RF frontend amplification
- Downconversion
- Digitalization
- Baseband signal processing

Figure 7 shows a block diagram of a generic receiver (source: *Global Positioning Systems Inertial Navigation and Integration*[9]).

2.5.1 *Antenna*

To receive as much signal from different satellites as possible the antenna must have a wide spatial angle, however if the gain varies too

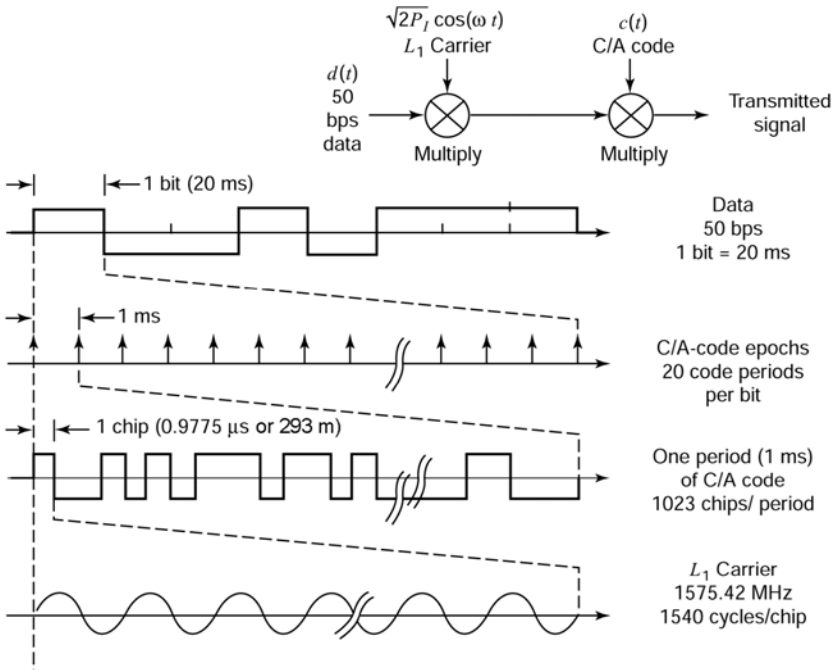

Figure 6: Structure of the L1 signal

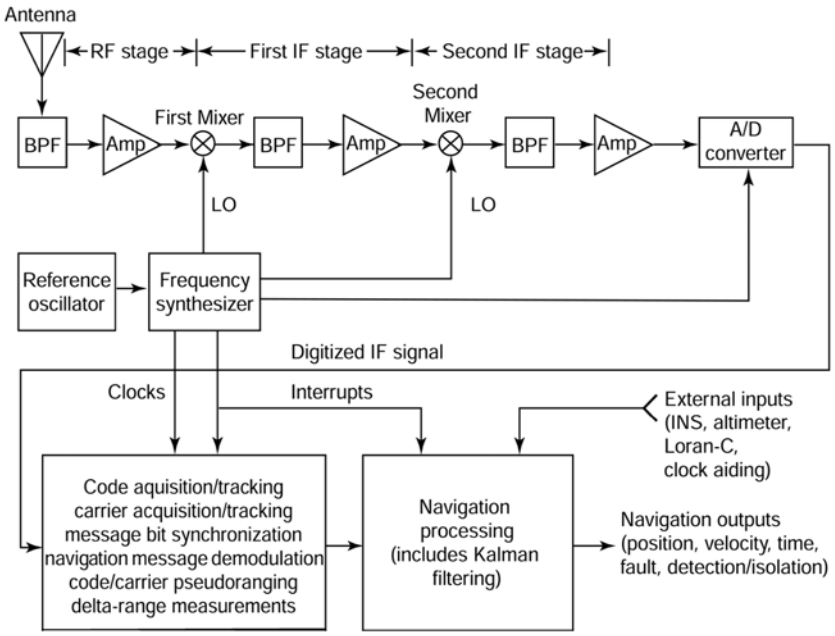

Figure 7: GPS receiver diagram

much with the angle the low-angle/low-gain signals may interfere with the strongest ones. Therefore the antenna design is a tradeoff between gain pattern and interference. An example of the gain pattern of a patch antenna is shown in figure 8 (source: Wikipedia).

Another aspect in antenna design is multipath: a signal reflected from a surface can be received if the antenna gain is wide enough,

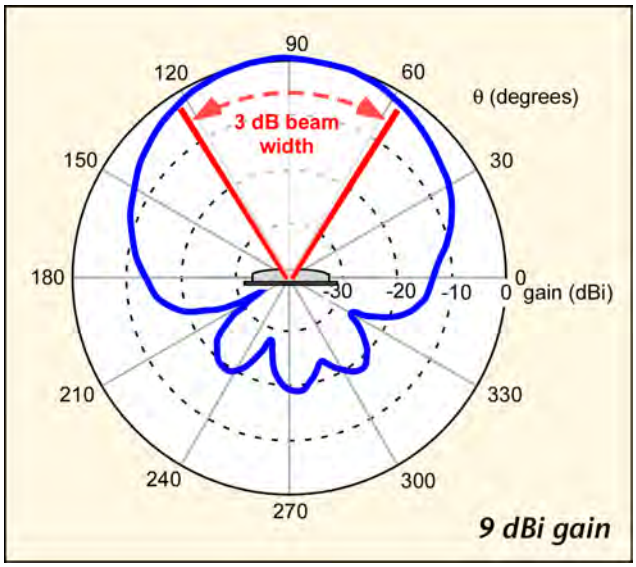

Figure 8: Typical patch antenna gain pattern

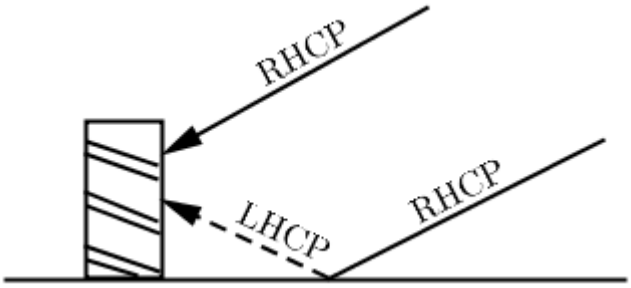

Figure 9: Effect of signal reflection on a Right Handed Circular Polarized antenna, the reflected signal is not received.

creating errors in position and above all attitude estimation. Because every reflection comes with a 180-degrees shift in signal polarization and the GPS signal itself has a right-handed circular polarization (RHCP), a RHCP antenna ignores all the signals coming from one reflection because they are LHCP (9); further reflections have usually lower strength. Alternatively the antenna can be shielded with metal rings of different diameters (choke ring), as shown in figure 10.

2.5.2 *RF frontend*

Through the Radio Frequency frontend the signal is both filtered and amplified, this is needed because the GPS signal power is very low and easily interfered by more powerful signals at adjacent frequency.

Figure 10: Choke ring around a GPS antenna, mitigating multipath effects (source: Trimble website).

2.5.3 *Downconversion*

In order to further amplify the signal its frequency must be lowered to one (single stage) or several (multistage) Intermediate Frequency (IF), this grants benefits from a filtering and Signal-to-Noise Ratio (SNR) aspects.

2.5.4 *Digitalization*

The Analog-to-Digital Converter (ADC) is used to sample and digitalize the signal, the frequency of this process must be chosen carefully in order to avoid aliasing and usually is several times the last IF value: without the downconversion of the signal the appropriate sampling frequency will be prohibitive.

2.5.5 *Baseband signal processing*

Once the signal is digitalized many different analysis can be performed, such as code phase tracking, carrier phase tracking and extraction of the Navigation Message. A space-based receiver has the disadvantage of a greater Doppler shift than a ground-based one, due to the high velocity of a LEO orbit (up to $8\mathrm{km/s}$); this complicates the signal tracking loop.

3

CARRIER PHASE DIFFERENTIAL GPS

SUMMARY

In this chapter various topics related to DGPS attitude determination are presented.

After the review of the various attitude parametrization alternatives the attitude determination problem is analysed, focusing on the QUEST algorithm; then the concept of Differential GPS attitude determination is presented and the related algorithms derived.

3.1 ATTITUDE PARAMETRIZATION

For the sake of attitude determination, as introduced in chapter 1, reference versors are required both in reference frame and in body frame. It is useful to define these reference frame, along with the means used to describe a spacecraft's attitude.

3.1.1 *Reference frames*

Figure 11 shows the roll-pitch-yaw (RPY) coordinates, used mainly for planet observation (also called nadir-pointing) spacecraft: the Z (yaw) axis is pointed towards nadir, the X (roll) axis is in the direction of the spacecraft's velocity and the Y (pitch) axis completes the left-handed frame. This reference frame will be used throughout this thesis.

The body frame is any left-handed frame that moves rigidly with the spacecraft, since most spacecrafts are similar to simple three di-

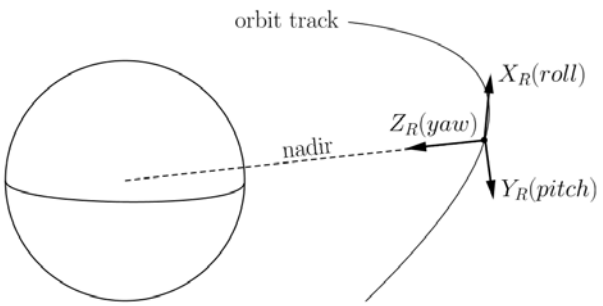

Figure 11: RPY coordinates

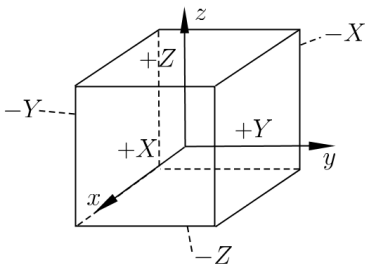

Figure 12: Body coordinates

mensional bodies the axis direction is used to refer to the spacecraft's outer panels (figure 12).

3.1.2 *Parametrization of rotation*

The rotations from reference to body frame can be parametrized in many ways (see table 3, adapted from Wertz's *Spacecraft Attitude Determination and Control* [2, p. 412]), the most used ones are Euler angles and quaternions.

3.1.2.1 *Euler angles*

Euler angles are defined as three successive rotations around the axis of four left-handed orthogonal triads, each triad is the result of the rotation of the previous one around one of its axis. It is common to name each sequence with the number of the axis that are to rotate, i.e. 1-2-3 means that the triad xyz is rotated around x and triad $x'y'z'$ is obtained, then a rotation about y' leads to $x''y''z''$, finally a rotation around z'' generates XYZ .

The most utilized sequences are 3-1-3 (precession-nutation-spin) for the description of the motion of spinning bodies such as spin-stabilized spacecraft, and 3-2-1 (yaw-pitch-roll) for the representation of attitude of three-axis stabilized spacecraft; for small rotations all the different sequences become similar.

One of the greatest downside of the Euler angles is that, since the rotation matrix contains trigonometric functions, some particular rotations can yield to a singularity in the rotation matrix: this phenomenon is called *gimbal lock* and force the algorithms using Euler angles to implement complex re-parametrization sequences if the attitude approach a gimbal lock condition.

3.1.2.2 *Quaternion*

A quaternion is a set of four parameters representing a rotation of θ about an axis $\widehat{X}$:

$$\overline{q} = \begin{Bmatrix} \mathbf{Q} \\ q \end{Bmatrix} = \begin{Bmatrix} \widehat{X}\sin(\theta/2) \\ \cos(\theta/2) \end{Bmatrix} \tag{1}$$

The quaternion is subject to a normalization condition:

$$\overline{q}^T\overline{q} = |\mathbf{Q}|^2 + q^2 = 1 \tag{2}$$

Having only one constraint is one of the advantages of this parametrization, the greatest one being that they have no singularities[1]. They are used mainly in attitude determination software for onboard computers.

3.1.2.3 *Gibbs vector*

Another parametrization than will be used in the subsequent section is the Gibbs vector. It is similar to the quaternion but composed only of three parameters:

$$Y = \widehat{X}\tan(\theta/2) = \frac{\mathbf{Q}}{q} \tag{3}$$

The Gibbs vector becomes infinite when $\theta = \pi$. It is possible to express the quaternion in terms of the Gibbs vector:

$$\overline{q} = \frac{1}{\sqrt{1+|Y|^2}} \begin{Bmatrix} Y \\ 1 \end{Bmatrix} \tag{4}$$

3.2 ORIGINAL ATTITUDE DETERMINATION PROBLEM

The main task in attitude determination is to find the rotation matrix between two coordinates frame, i.e. $\mathbf{v}_b = R_a^b\mathbf{v}_a$ (R_a^b is the rotation matrix from frame a to frame b), given a set of n measurements. If $\widehat{V}_i$ is the i-th versor in reference frame and $\widehat{W}_i$ the i-th versor in body frame, the attitude or rotation matrix A satisfy the relationship:

$$\widehat{W}_i = A\widehat{V}_i \qquad \text{for } i = 1..n \tag{5}$$

1 For a deeper discussion of quaternions see *Spacecraft Attitude Determination and Control* [2, appendix D]

Table 3: Representation of attitude

Parametrization	Advantages	Disadvantages	Common applications
Direction cosine matrix	No singularities, no trigonometric functions, convenient product rule for successive rotations	Six redundant parameters	Analysis
Euler axis and angle	Clear physical interpretation	One redundant parameter, axis undefined when $\sin\phi = 0$, trigonometric functions	Commanding slew manoeuvres
Euler angles	No redundant parameters, physical interpretation is clear in some cases	trigonometric functions, singularity at some θ, no convenient product rule for successive rotations	Analytic studies, input/output, onboard attitude control of 3-axis stabilized spacecraft
Gibbs vector	No singularities, no trigonometric functions, convenient product rule for successive rotations	Infinite for 180 deg rotations	Analytic studies
Quaternion	No singularities, no trigonometric functions, convenient product rule for successive rotations	One redundant parameter, no obvious physical interpretation	Onboard inertial navigation

However if the measurements are affected by errors the attitude matrix is not unique.

At first only a deterministic solution for pairs of measurements was available, where part of the measurements were discarded and the attitude matrix computed in a non-optimal way; one example being the TRIAD algorithm[10] based on the algebraic solution. Where more than two measurements are available, such as with star trackers measurements, the algorithm needs to run with every pair of measurements and then the attitude matrix is obtained by combining the single results.

In order to find an optimal solution it is useful formulate the problem in terms of a loss function, as proposed by Whaba[11]:

$$L(A) = \frac{1}{2}\sum_{i=1}^{n} a_i |\widehat{W}_i - A\widehat{V}_i|^2 \tag{6}$$

The minimization of $L(A)$ is complicated by the six constraints of the attitude matrix A: this is because A is required to be an orthonormal matrix, i.e. its rows and column are orthogonal and with unitary norm ($A^T A = AA^T = I$ where I is the identity matrix).

By parametrizing the attitude matrix with quaternions (q-method) Davenport[12] reduces the constraints from six to one, namely the normalization of the quaternion; furthermore it success in turning the quadratic loss function into a eigenvalue problem.

The solution of a four-dimensional eigenvalue problem can be computational heavy, especially if attitude is rapidly changing and the algorithm has to run several times per second; nonetheless this is an accurate alternative when attitude estimation is seldom needed.

An approximated solution of Whaba's loss function parametrized with quaternions is proposed by Shuster[10], where the eigenvalues are found using a Newton-Raphson iterative scheme. This algorithm, named QUEST (QUaternion ESTimator), allows much faster computations while being an optimal solutor.

Other than QUEST other algorithms exist, such as Markley's SVD[13] and FOAM[14], Mortari's ESOQ[15] and ESOQ-2[16]. They differ in terms of speed and accuracy[1], some of them are suited for application when the sensor used have very different accuracies, such as star trackers and sun sensors. Figure 13 present a speed comparison for different algorithms, in terms of number of floating point operations for each run.

While a thorough derivation of QUEST algorithm can be found in Shuster's article, it is useful to outline it main steps as it will be implemented later. At first the quaternion parametrization will be shown,

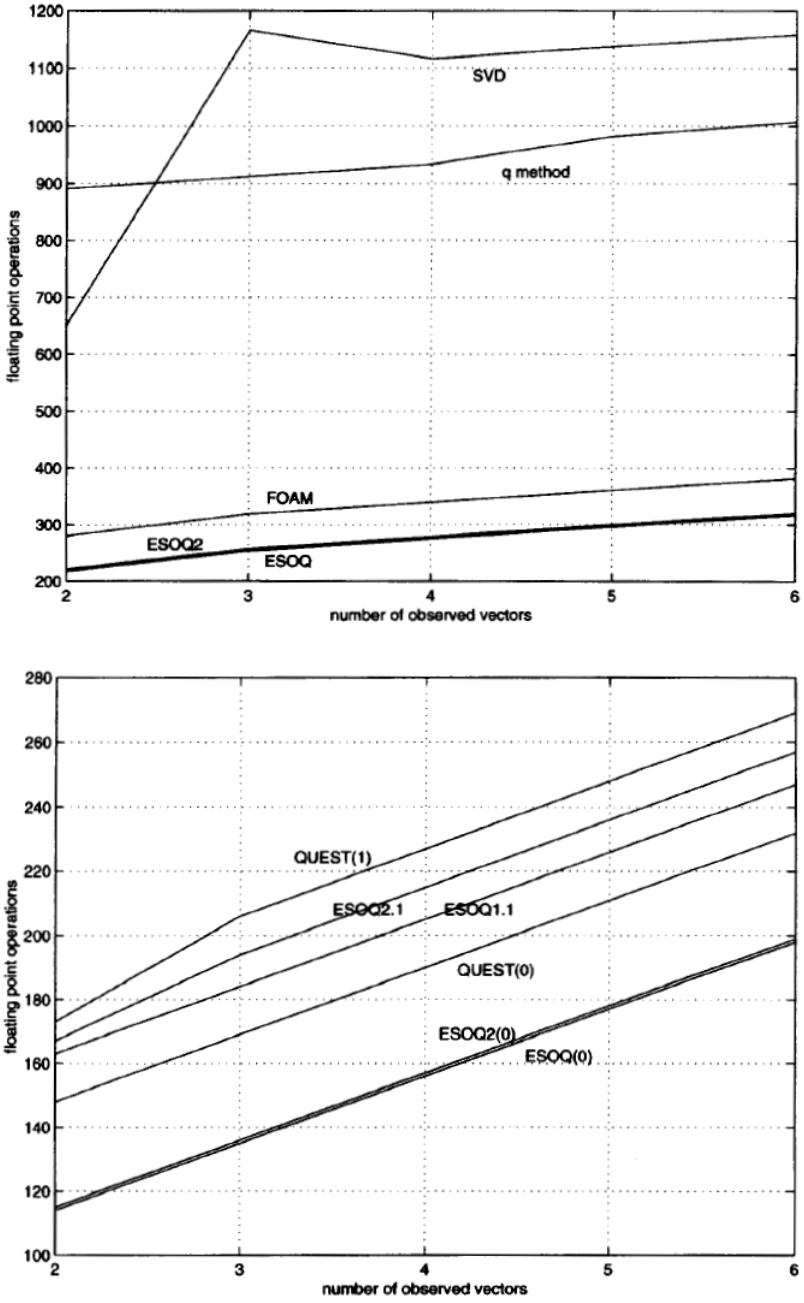

Figure 13: Speed comparison[1] for robust estimation (q-method and SVD, top figure) and fast estimation algorithms (QUEST and ESOQ, bottom figure)

following Davenport, then the proper QUEST algorithm will be presented.

3.2.1 *Quaternion parametrization*

It is possible to write the loss function 6 as a gain function $g(A)$, then writing the Froebenius norm with the trace operator [2]:

$$g(A) = 1 - L(A) = \sum_{i=1}^{n} a_i \widehat{W}_i^T A \widehat{V}_i = tr(AB^T) \tag{7}$$

where B is the *attitude profile matrix*.

$$B = \sum_{i=1}^{n} a_i \widehat{W}_i \widehat{V}_i^T \tag{8}$$

As stated earlier the quaternion parametrization is used in order to bring down the number of constraints from six to one; it is possible to write the attitude matrix as a function of the quaternion $\overline{q}$:

$$A(\overline{q}) = (q^2 - \mathbf{Q} \cdot \mathbf{Q})I + 2\mathbf{Q}\mathbf{Q}^T + 2q\underline{Q} \tag{9}$$

$$\underline{Q} = \begin{bmatrix} 0 & -Q_3 & Q_2 \\ Q_3 & 0 & -Q_1 \\ -Q_2 & Q_1 & 0 \end{bmatrix} \tag{10}$$

This allows to write the gain function as:

$$g(\overline{q}) = (q^2 - \mathbf{Q} \cdot \mathbf{Q})tr(B^T) + 2tr(\mathbf{Q}\mathbf{Q}^T B^T) + 2qtr(\underline{Q}B^T) \tag{11}$$

Making use of the definition of quaternion:

$$g(\overline{q}) = \overline{q}^T K \overline{q} \tag{12}$$

K is a 4x4 matrix:

$$K = \begin{bmatrix} S - \sigma I & Z \\ Z^T & \sigma \end{bmatrix} \tag{13}$$

2 $\|A\|_F^2 = \|P^T B P\|_F^2 = tr((P^T B P)(P^T B P)) = tr(BB^T) = \|B\|_F^2$

where the different quantities are such defined:

$$\sigma = tr(B) \sum_{i=1}^{n} a_i \widehat{W}_i \cdot \widehat{V}_i \tag{14}$$

$$S = B + B^T = \sum_{i=1}^{n} a_i (\widehat{W}_i \widehat{V}_i^T + \widehat{V}_i \widehat{W}_i^T) \tag{15}$$

$$Z = B - B^T = \sum_{i=1}^{n} a_i (\widehat{W}_i \times \widehat{V}_i) \tag{16}$$

Equation 12 must be maximized while being subjected to the normalization condition of the quaternion.

The Lagrange multipliers method allows to solve a constrained maximization problem introducing n scalar constants, where n is the number of constraints. The Lagrangian function is then formulated by adding to the original function the constraints:

$$g(\overline{q}') = \overline{q}^T K \overline{q} - \lambda \overline{q} \overline{q}^T \tag{17}$$

λ is the Lagrange multiplier. Maximization is achieved through derivation:

$$K\overline{q} = \lambda \overline{q} \tag{18}$$

This is the definition of an eigenvector problem, so $\overline{q}$ must be an eigenvector of K and λ its related eigenvalue. Substituting equation 18 back into equation 12 leads to

$$g(\overline{q}) = \overline{q}^T K \overline{q}) = \lambda \overline{q}^T \overline{q} = \lambda \tag{19}$$

It is straightforward that the maximum value of $g(\overline{q})$ will be obtained for the maximum eigenvalue λ. It is therefore proven that the original Whaba's maximization problem 6 is reduced to the search of the maximum eigenvalue of the K matrix, or:

$$K\overline{q}_{opt} = \lambda_{max} \overline{q}_{opt} \tag{20}$$

3.2.2 *Eigenvalues estimation*

From the definition of the K matrix 13 and the quaternion 3 it is possible to formulate equation 18 as a set of two separated equations:

$$\begin{bmatrix} S-\sigma I & Z \\ Z^T & \sigma \end{bmatrix} \begin{Bmatrix} \mathbf{Q} \\ q \end{Bmatrix} = \lambda \begin{Bmatrix} \mathbf{Q} \\ q \end{Bmatrix} \tag{21}$$

$$\begin{cases} [S-(\sigma+\lambda)I]\mathbf{Q} + Zq = 0 \\ Z^T\mathbf{Q} + (\sigma-\lambda)q = 0 \end{cases} \tag{22}$$

$$\begin{cases} Y = \frac{\mathbf{Q}}{q} = [(\sigma+\lambda)I]^{-1}Z \\ \lambda = \sigma + \frac{\mathbf{Q}}{q}Z = \sigma + YZ \end{cases} \tag{23}$$

Substituting the expression for Y in the very last equation leads to:

$$\lambda = \sigma + Z^T \frac{1}{[(\lambda+\sigma)I - S]} Z \tag{24}$$

As stated before the Gibbs vector becomes infinite for a rotation of π, so this expression is invalid near that rotation: this coincide with the matrix $[(\lambda+\sigma)I - S]$ becoming singular.

The goal now is to find an approximate solution of the characteristic equation, similar to equation 24, expressed with quaternions.

The Cayley-Hamilton theorem states that every square matrix over a commutative ring satisfies its own characteristic equation. If M is a square matrix its characteristic equation is:

$$\det|M - \lambda I| = 0 \tag{25}$$

where det is the determinant and λ an eigenvalue of the matrix M. Expanding this expression:

$$
\begin{aligned}
&\det\begin{bmatrix} M_{11}-\lambda & M_{12} & M_{13} \\ M_{21} & M_{22}-\lambda & M_{23} \\ M_{31} & M_{32} & M_{33}-\lambda \end{bmatrix} = \\
&= (M_{11}-\lambda)(M_{22}-\lambda)(M_{33}-\lambda) + M_{12}M_{23}M_{31} + M_{13}M_{21}M_{32} \\
&\quad -(M_{22}-\lambda)M_{31}M_{13} - (M_{11}-\lambda)M_{23}M_{32} - (M_{33}-\lambda)M_{21}M_{12} \\
&= -\lambda^3 + \underbrace{\lambda^2(M_{11}+M_{22}+M_{33})}_{tr(M)} \\
&\quad + \underbrace{\lambda(-M_{11}M_{22} - M_{22}M_{33} - M_{11}M_{33} + M_{31}M_{13} + M_{32}M_{23} + M_{21}M_{12})}_{tr(adj(M))} \\
&\quad + \underbrace{M_{11}M_{22}M_{33} + M_{12}M_{23}M_{31} + M_{13}M_{21}M_{32}}_{det(M)} \\
&\qquad \underbrace{-M_{22}M_{31}M_{13} - M_{11}M_{32}M_{23} - M_{33}M_{21}M_{12}}_{det(M)} \qquad (26)
\end{aligned}
$$

where the tr is the trace and adj is the classical adjoint (or adjugate), i.e. the transpose of the cofactor matrix[3].

$$-\lambda^3 + tr(M)\lambda^2 - tr(adj(M))\lambda + det(M) = 0 \qquad (27)$$

Applying the Cayley-Hamilton to the last equation:

$$-M^3 + tr(M)M^2 - tr(adj(M))M + det(M)I = 0 \qquad (28)$$

Defining the following quantities equation 28 becomes:

$$\sigma = tr(M) \qquad k = tr(adj(M)) \qquad \Delta = det(M) \qquad (29)$$

$$-\lambda^3 + \sigma\lambda^2 - k\lambda + \Delta = 0 \qquad (30)$$

By the definition of C-H theorem M can be any square matrix, if $M = [(\lambda+\sigma)I - S]$:

$$[(\lambda+\sigma)I - S]^{-1} = \gamma^{-1}(\alpha I + \beta S + S^2) \qquad (31)$$

where

$$\alpha = \lambda^2 - \sigma^2 + k \qquad \beta = \lambda - \sigma \qquad \gamma = (\lambda+\sigma)\alpha - \Delta \qquad (32)$$

3 The elements of the cofactor matrix are $C_{ij} = (-1)^{i+j}m_{ij}$, where m_{ij} is the minor of the M matrix relative to the i-th row and j-th column, i.e. the determinant of the matrix obtained by removing from M the i-th row and j-th column.

Substituting equation 31 back into the expression for the eigenvalues derived earlier (equation 24) leads to:

$$\lambda^4 - (a+b)\lambda^2 - c\lambda + (ab + c\sigma - d) = 0 \tag{33}$$

$$a = \sigma^2 - K \qquad b = \sigma^2 + Z^T Z \qquad c = \Delta + Z^T S Z \qquad d = Z^T S^2 Z \tag{34}$$

Finally a simplified equation for the eigenvalues is derived. Equation 33 can be solved with an iterative method, such as Newton-Raphson method. This is particularly convenient because the method needs a starting value for λ, but $\lambda = g(A)$ (equation 19) and since $g(A)$ is to be maximized, the initial guess can be $\lambda_{max} = 1$.

Once the value for λ_{max} is obtained the only thing left is calculating the attitude quaternion. Again from equation 31 and 4, substituting $\lambda = \lambda_{max}$:

$$\overline{q}_{opt} = \frac{1}{\sqrt{\gamma^2 + |X|^2}} \begin{Bmatrix} X \\ \gamma \end{Bmatrix} \tag{35}$$

where

$$X = (\alpha I + \beta S + S^2) Z \tag{36}$$

Figure 14 summarises the QUEST algorithm main steps and the related quantities.

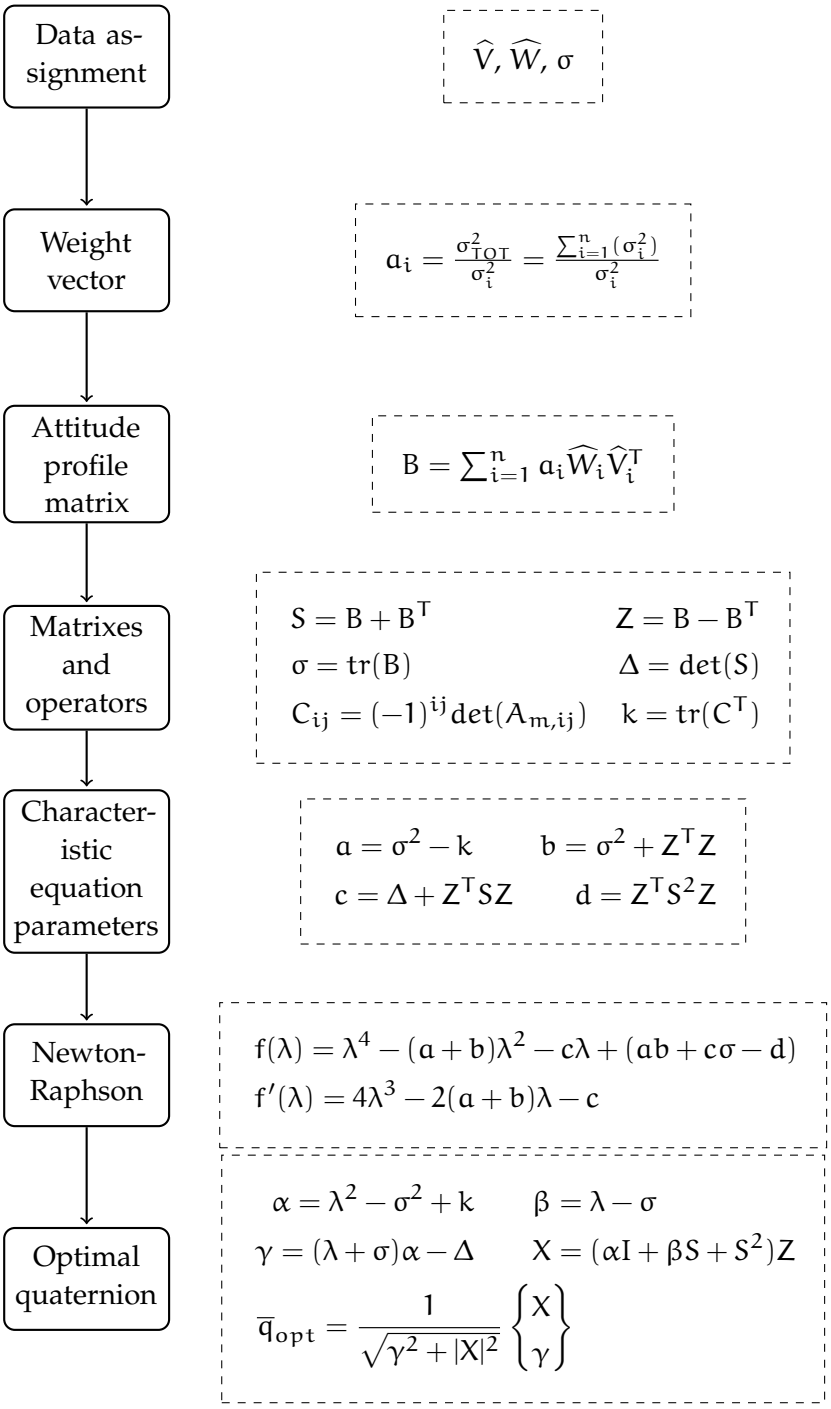

Figure 14: QUEST algorithm block diagram

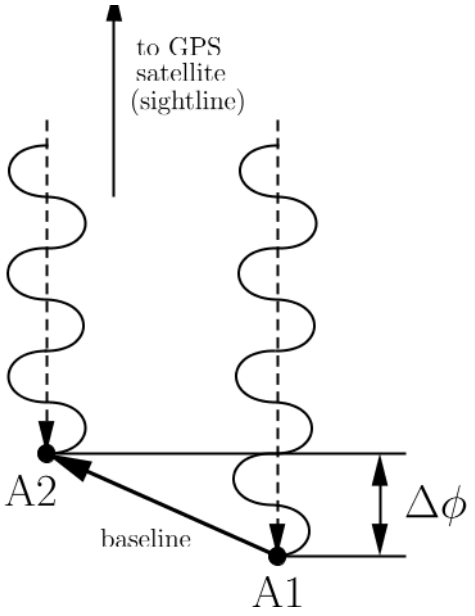

Figure 15: The phase difference of the signal received from two antennas

3.3 DGPS CONCEPT

Differential GPS techniques make use of multiple receivers in order to augment the precision of the reconstructed position and are the focal point in GPS attitude determination.

Using an appropriate tracking loop it is possible to measure the phase of the GPS signal carrier, the difference between measurement taken by different antennas is proportional to their relative range with respect to the observed GPS satellite.

The phase difference between the signal received from two antennas is outlined in figure 15; from the figure it can be noted easily that the phase difference $\Delta\phi$ is comparable to a length, the distance traveled is $r = \lambda\Delta\phi$ where λ is the wavelength of the carrier.

If the relative position of the antennas is fixed, i.e. they are mounted on a rigid body, the relative range is also proportional with the angle between the vector connecting the antennas, or baseline, $\mathbf{b}$ and the GPS satellite line of sight $\mathbf{s}$.

The phase difference measure $\Delta\phi^0$ is related to the relative range Δr and the angle θ by:

$$\Delta r = b_l \cos\theta = \lambda\frac{\Delta\phi^0}{2\pi} \tag{37}$$

Figure 16 represents the baseline and sightline versors with respect to the signal incoming from a GPS satellite, the incoming waveform is planar because of the great distance between the emitter and the

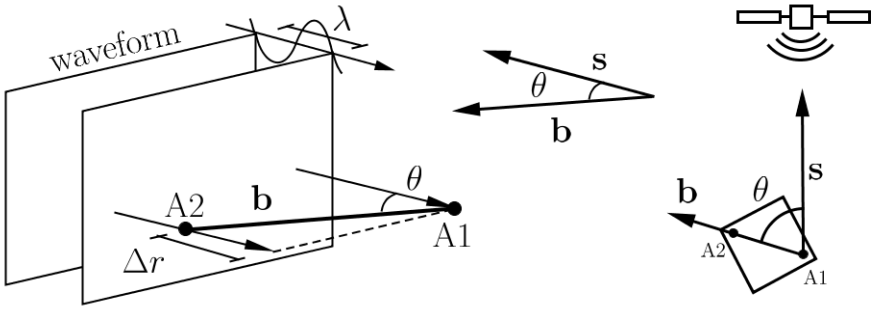

Figure 16: Concept scheme of two antennas DGPS

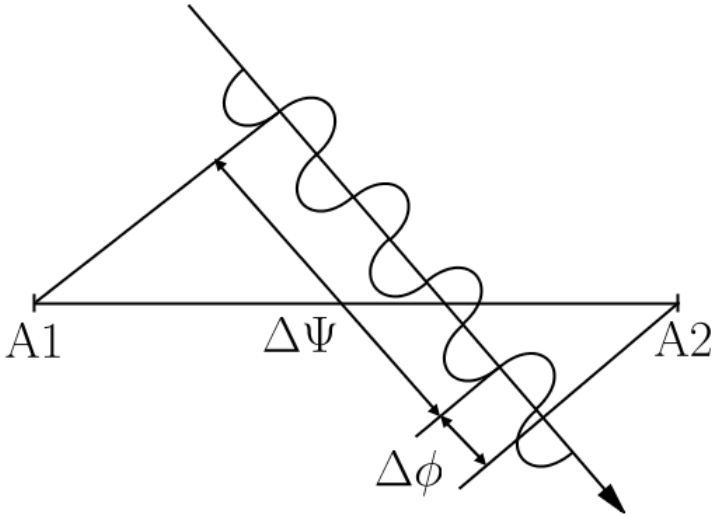

Figure 17: Integer ambiguity

receiving antennas.

If the baseline length b_l is longer than the wavelength of the carrier the phase measurement $\Delta\psi$ is formed by two components: a number of integer wavelength n and the actual phase difference; this leads to an ambiguity when computing the angle that needs to be resolved with other methods. With this consideration the previous equation becomes:

$$\Delta r = b_l \cos\theta = \lambda\left(n + \frac{\Delta\phi^0}{2\pi}\right) \tag{38}$$

$$\Delta\psi = 2\pi n + \Delta\phi^0 \tag{39}$$

It is possible, making use versor notation for the baseline and sightline versors $\mathbf{b}$ and $\mathbf{s}$ with no integer ambiguity, to define the normalized phase difference measurement $\Delta\phi$:

$$\Delta\phi = \frac{\lambda\Delta\phi^0}{2\pi b_l} = \mathbf{b}^T\mathbf{s} \tag{40}$$

From this definition it is evident that the normalized phase difference $\Delta\phi$ is the direction cosine of the two versors; this relationship is valid for all the reference frames, provided that the same frame is used for expressing both $\mathbf{b}$ and $\mathbf{s}$.

3.4 GPS ATTITUDE DETERMINATION

The GPS measurements introduce another aspect in attitude determination: the phase difference is not a vector but a scalar, and vectorized measurements are needed in order to use attitude estimation algorithm such as QUEST.

In the conversion of phase difference measure to vectorized measures equation 40 is a central point, following Crassidis and Markley[17]. The two versors groups, sightlines and baselines, can be expressed in both the reference and the body frame; of these four quantities two are known:

- sightlines in reference frame $\mathbf{s}_b$, determined from knowledge of the spacecraft and GPS constellation orbit positions
- baselines in body frame $\mathbf{b}_r$, known from spacecraft design

The other two are to be obtained by converting the scalar phase differences; the problem can be stated in two ways, both of them taking the steps from equation $\Delta\phi = \mathbf{b}^T\mathbf{s}$:

1. determining sightlines in body frame $\mathbf{s}_b$ leads to $\Delta\phi = \mathbf{b}_b^T\mathbf{s}_b$
2. determining baselines in reference frame $\mathbf{b}_r$ leads to $\Delta\phi = \mathbf{b}_r^T\mathbf{s}_r$

From any these two equation a cost function can be written and minimized by derivation. These two ways pose different but equally strong design constraints over the antennas layout geometry: the former requires at least three non-coplanar baselines, while the latter a at least three non-coplanar sightlines.

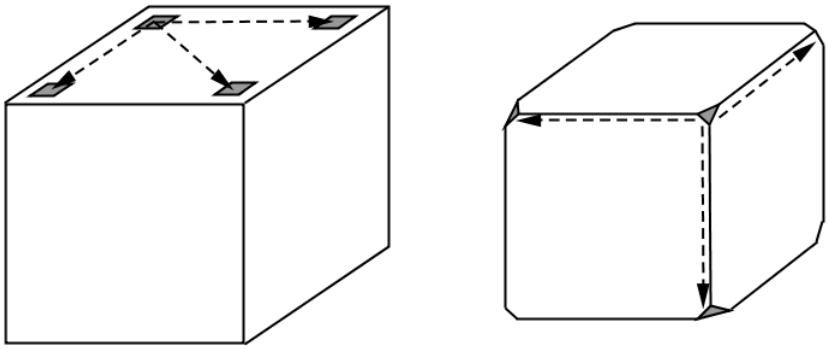

Figure 18: Examples of antenna geometry: on the left they are arranged in a coplanar fashion, non compatible with equation 42

3.4.1 *Sightlines in body frame*

The first cost function, expressed in body coordinates, is:

$$J_j(\mathbf{s}_j) = \frac{1}{2}\sum_{i=1}^{m}\frac{1}{\sigma_{ij}^2}(\Delta\phi_{ij} - \mathbf{b}_i^T\mathbf{s}_j)^2 \qquad \text{for } j = 1..n \tag{41}$$

where n is the number of observed GPS satellites (number of sightlines), m is the number of available baselines and σ_{ij}^2 is the covariance of the measurement process. The inverse of the covariance $\frac{1}{\sigma_{ij}^2}$ is the equivalent of the weight a_i in equation 6. Minimization of this cost function leads to:

$$\mathbf{s}_j = M_j^{-1}y_j \tag{42}$$

where

$$M_j = \sum_{i=1}^{m}\frac{1}{\sigma^2}\mathbf{b}_i\mathbf{b}_i^T \quad y_j = \sum_{i=1}^{m}\frac{1}{\sigma^2}\Delta\phi_{ij}\mathbf{b}_i \qquad \text{for } j = 1..n \tag{43}$$

The major consequence of this approach is that *at least three non-coplanar baselines are required*: this has a great influence on the system's design, as shown in figure 18.

3.4.2 *Baselines in reference frame*

Developing the same solution expressing the baselines in reference frame leads to the following equations:

$$J_i(\mathbf{b}_i) = \frac{1}{2}\sum_{j=1}^{n}\frac{1}{\sigma_{ij}^2}(\Delta\phi_{ij} - \mathbf{b}_i^T\mathbf{s}_j)^2 \qquad \text{for } i = 1..m \tag{44}$$

It is worth pointing out that now the sum is over the n sightlines, while all these equation are in reference frame. Minimization leads to:

$$\mathbf{b}_i = N_i^{-1} z_i \tag{45}$$

where

$$n_i = \sum_{j=1}^{n} \frac{1}{\sigma^2} \mathbf{s}_j \mathbf{s}_j^T \quad z_i = \sum_{j=1} n \frac{1}{\sigma^2} \Delta\phi_{ij} \mathbf{s}_j \qquad \text{for } i = 1..m \tag{46}$$

As anticipated before, the constraint posed by equation 45 is that *at least three non-coplanar sightlines are required*. This is a less restraining condition than the first one, since the orbital position of the GPS constellation, with satellite spread over six orbital planes, renders this event impossible.

After the calculation of either sightlines in body frame or baselines in reference frame the conversion from scalar to vector is achieved, the attitude can be estimated with a standard determination algorithm such as QUEST, using as inputs either sightlines (case 1) or baselines (case 2).

4 SIGNAL AVAILABILITY

SUMMARY

The first concern regarding DGPS in space application is signal availability: while the GPS constellation is designed to provide a minimum number of six satellites visible from any point on Earth surface, this number drops as the altitude of the receiving platform rises.

Two different antenna layouts will be evaluated for different orbit altitudes and antenna gain characteristics.

4.1 SIMULATION PARAMETERS

The number of visible GPS satellites is a major factor in DGPS attitude determination; a minimum number of three is the requirement for the second attitude determination algorithm shown in the previous chapter. More than three satellites will improve the attitude estimation, so the number of available satellites is a first measure of the system's overall accuracy.

The signal availability is influenced by the following factors:

- orbit geometry
- GPS antenna emission power and radiation pattern
- receiving antenna radiation pattern and layout geometry

4.1.1 *Orbit geometry*

GPS satellites are positioned along six orbital planes, each one with an inclination of 55° and with a separation of 60°. Originally four satellites per plane were operative for a total of 24, but this number has increased to 32 to improve precision and availability.

The orbit altitude is 20200km to grant a semi-synchronous period, i.e. the orbit period is half a sidereal day.

The GPS almanac data are available on the Navigation Center site of U.S. Department for Homeland Security[1], for every GPS week and in various formats. An example of an entry of the YUMA almanac is shown in table 4. The satellites position for the same almanac data are represented in figure 19.

1 http://www.navcen.uscg.gov/?pageName=gpsAlmanacs

Table 4: The YUMA entry for satellite 01, week number 761 (October 2013)

******** Week 761 almanac for PRN-01 ********	
ID:	01
Health:	000
Eccentricity:	0.2826213837E-002
Time of Applicability(s):	319488.0000
Orbital Inclination(rad):	0.9609934236
Rate of Right Ascen(r/s):	-0.7760323249E-008
SQRT(A) (m 1/2):	5153.638184
Right Ascen at Week(rad):	-0.5683245271E+000
Argument of Perigee(rad):	0.332184364
Mean Anom(rad):	0.1340404472E+001
Af0(s):	0.5722045898E-005
Af1(s/s):	0.0000000000E+000
week:	761

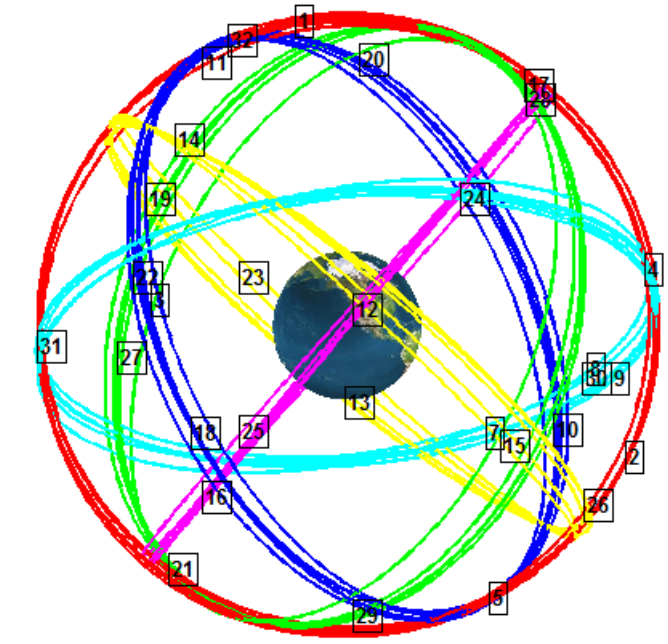

Figure 19: GPS satellites position relative to the GPS YUMA almanac, week 761

4.1.2 *GPS antenna*

The next subjects of analysis are GPS spacecraft's antenna power and radiation pattern. While the former is not an issue, due to the fact that an orbiting spacecraft is usually closer to the signal source than a ground user and it doesn't have to deal with atmospheric disturbances, the latter becomes more and more influential as the altitude increase. Extensive analysis of the link budget for a spacecraft-based GPS receiver are performed in [**?**] and show that the available power on orbit is equivalent or better than on the ground.

The gain of an antenna, i.e. the power of the signal of the antenna compared with the power irradiated from an isotropic antenna, is a function of the direction. A generic radiation pattern is shown in figure 20 and its main element outlined: the signal amplification is measured in decibel (dB), the main lobe corresponds to the main emitting/receiving direction of the antenna and the half-power bandwidth is the arc inside which the gain is inside a -3dB range with respect to the maximum gain, this corresponds to a half-power condition [18].

While the specific characteristics of the antennas depend on the type of GPS satellite, some are very similar. The antenna emission pattern is designed in order to grant an uniform power throughout all the visible Earth surface, the irradiation towards space is minimized and often due to side lobes.

The semi aperture of the main lobe for the L1 signal is $\sim 21.3°$ [19] and this value is used as a cut-off for the simulation, meaning that any signal from the side lobes is going to be ignored.

It is evident from figure 21 that this is not a factor for low earth orbits satellites, the range of altitude from 0 to 3000 km being covered; in order to evaluate GPS availability for higher orbits such analysis is required[20].

4.1.3 *Receiving antenna*

Two types of antennas are considered: patch and helix (see figure 22), each antenna type corresponds to a different antenna layout that is designed to take advantage of each antenna's characteristics. The layouts are:

- four patch antennas mounted on the same panel (figure 23a)
- four helix antennas mounted on the edges of the spacecraft (figure 23b)

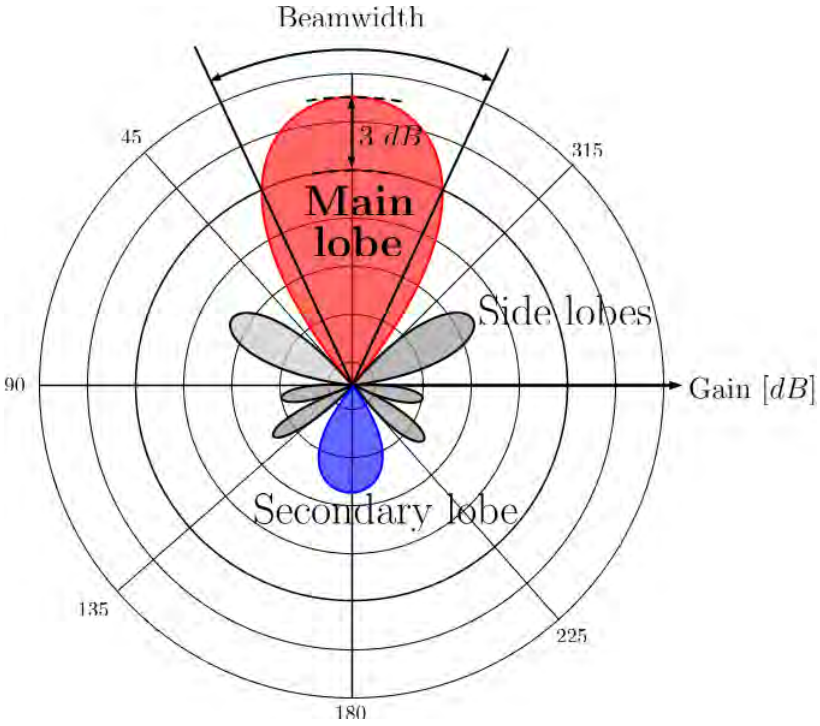

Figure 20: Polar diagram of a generic radiation pattern

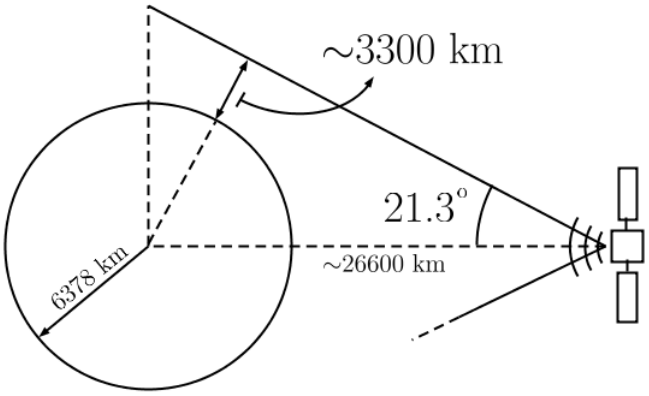

Figure 21: GPS signal main lobe

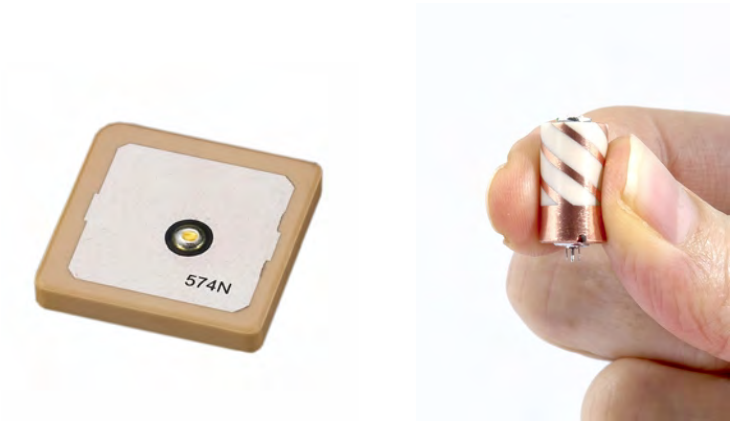

Figure 22: Patch and helix antennas, the patch antenna is 25x25x4.5 mm

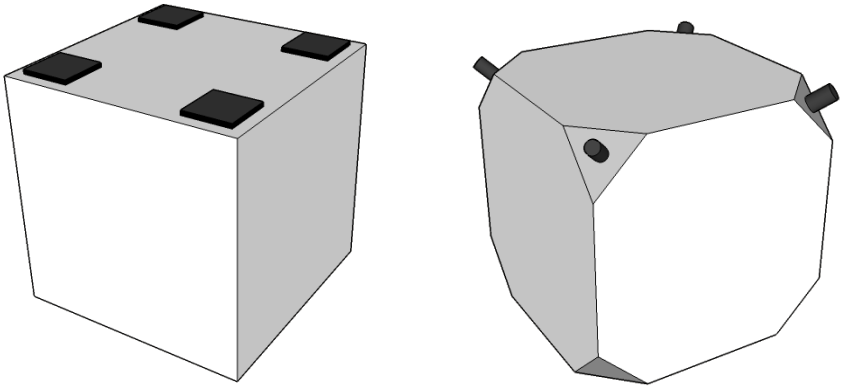

(a) Patch (b) Helix

Figure 23: The two proposed layouts

In order to maximize the visibility the antennas are pointed to the zenith panel (−Z with respect to figure 12), the spacecraft is considered nadir-pointing.

4.1.3.1 *Patch*

Patch antennas are usually more economic and have higher gain, however the gain decreases for signals with low incidence angle and the gain pattern itself is very sensitive to the extension and shape of the mounting surface.

This layout is the simplest one from a mechanical point of view and is the most compatible with the Cubesat design. Mounting the antenna on a large surface tends to raise the gain near the zenith and create a more directional radiation pattern, while the opposite is true for smaller surfaces.

It is difficult to take into account properly the radiation pattern due to mounting near to the edges of the plane, as shown in figure 23a,

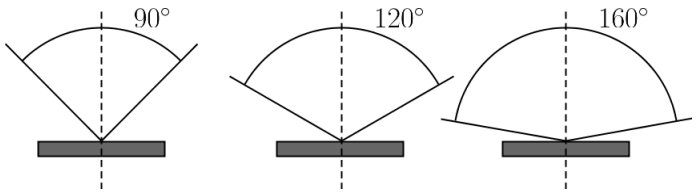

Figure 24: Patch antenna beamwitdh

because its shape is a result of a combination of the two opposite effects described previously [21].

In order to achieve a meaningful result the radiation pattern is modelled as a step function, which is 1 (signal received) inside the detection threshold and 0 (signal ignored) outside. While this is a rather simplistic approach, a more in-depth simulation of the link would have required not only precise information about the layout's radiative characteristics, that due to the effects explained before are obtainable only with tests of the chosen antennas and surface combination, but also a complete implementation of a GPS receiver in all its functions [22]. This approach is also used for the attitude performance evaluation of the RADCAL experiment[4], and can give some meaningful insight on the layout design choices and also a requirement prediction for the complete DGPS sensor.

For the patch antenna the detection threshold (beamwidth) is set to different values throughout the simulations: 90° (worst case), 120° (mid case) and 160° (best case). The 180° case has not been considered due to antenna to antenna geometric masking.

4.1.3.2 *Helix*

Helix antennas have lower gain but their gain pattern is more uniform; an helix antenna is often polarized: as introduced before this helps in the rejection of multipath signals.

Helix antennas are less influenced by the ground plane [21], the proposed layout is intended to take advantage of their rather omnidirectional gain pattern to acquire a greater number of GPS signals; however it doesn't fit the Cubesat standards as well as the previous design and the helix antenna itself has a greater geometric envelop than the more compact patch antenna.

Two cases have been analysed: an optimum case where the antenna is able to receive with a beamwidth of 260°, this restriction being imposed by the geometry of the spacecraft's panels, and a worst case with a beamwidth of 180°, where the ground plane limits the field

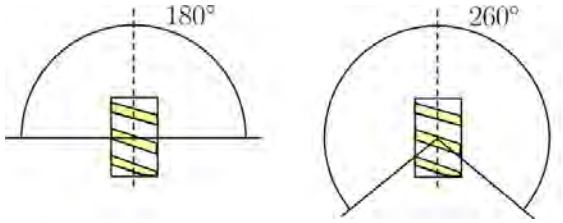

Figure 25: Helix antenna beamwitdh

of view; the latter case is useful to evaluate the performance of this layout as if patch antenna were used.

4.2 SIMULATION RESULTS

The simulations involve a 24 hours period with a time discretization of 10 s, with the GPS ephemeris data taken from the YUMA almanac of week 761 (see table 19). The spacecraft's orbits considered are circular, with an altitude ranging from 300 to 3000 km; the orbital inclination is 0° but this is irrelevant for this simulation, as will be shown later. The spacecraft is nadir-pointing and the GPS antenna are positioned in the $-Z$ (zenith) direction.

The results are presented in terms of:

- number of visible satellites (time history and cumulative graph over 24 hours)
- availability windows and average availability time

At first some general remarks about the DGPS system are presented, with particular respect to the receiver performance requirements that the space application poses; then the single layouts analysis are detailed.

4.2.1 *General considerations*

Figure 26 shows a representation of the intervals of time when each GPS satellite is visible by the antenna set. The number on the right of each interval is its duration in seconds.

While figure 26 displays the results for a single simulation, tables 5 and 6 summarise the average satellite availability time for all the simulations performed.

This is an important indication because the receiver's tracking software needs to be designed in order to acquire the GPS signal in a short period of time, the average satellite availability time ranging from 10 to 30 minutes for a satellite orbiting at an altitude of 300 km. It has been proved [23] that using specifically designed algorithm implemented in an FPGA (Field Programmable Gate Array) integrated

circuit it is possible to lower the acquisition time from several tens of minutes to three minutes or less; this is a key aspect in order to exploit at best the available signals.

Figure 27 represents the time history of the number of visible satellites. The graph is very "jumpy", this means that a lot of different satellites come quickly in and out of view: the receiving hardware and software need to be fast and flexible in order to manage the acquisition process; again from [23] the use of FPGA technology allows a greater deal of flexibility than standard integrated circuits.

Inclination is not an important factor, this is evident from figure 28 and is an expected result because of the inherent design of the GPS constellation. All the simulations are therefore performed with i=0°.

4.2.2 *Patch*

Figures 29, 30 and 31 summarize the number of visible satellites in a cumulative graph, one for each antenna beamwidth.

The generalized tendency is that higher orbits have a lower number of visible satellites, so the use of DGPS becomes more and more difficult increasing the altitude; moreover the 90° beamwidth case (figure 29) is not promising because of the possibility that least than three satellites are into view: in these periods of time, a total of 6 hours per day at 300 km and 12 hours at 3000 km, the DPGS attitude measure is not available.

Thus a patch antenna beamwidth of 120° or more is recommended in order to achieve an attitude determination solution for the major part of an orbit.

4.2.3 *Helix*

The helix antenna layout will be now analyzed. From table 6 and figure 32 is evident that the 180° beamwidth is not a viable solution, because of the low number of the visible satellites. The other configuration (figure 33) has very similar results with the 160° patch antenna: while the helix antenna has a far greater beamwidth than the patch antenna, the need for the satellite to be visible by all the antennas renders irrelevant this advantage.

This results, together with the mechanical complications of the helix antenna layout, make the patch antenna configuration the most suitable for a Cubesat-like miniature satellite.

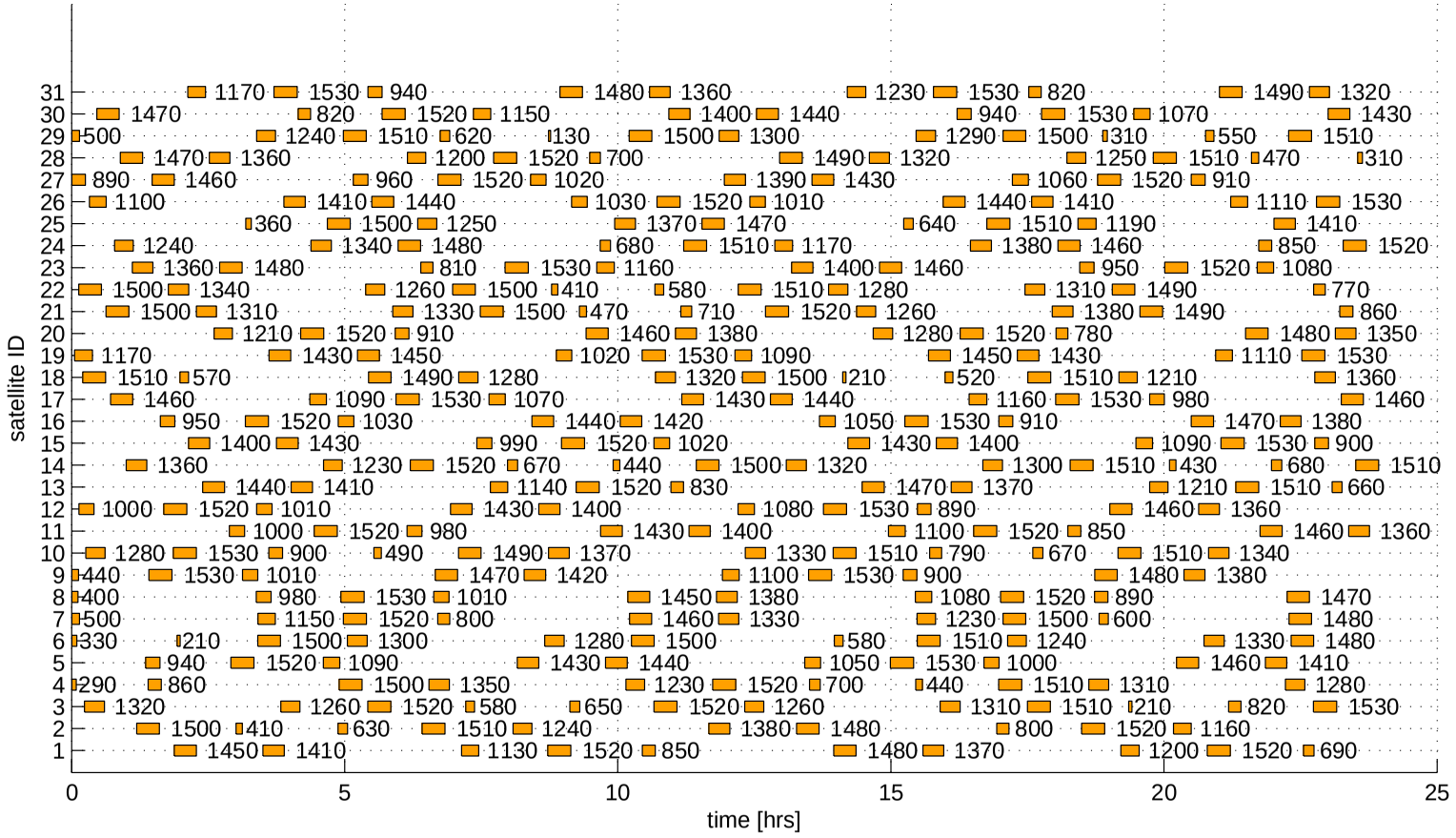

Figure 26: Satellite visibility history, patch antenna, bw=120°, alt=300km

Table 5: Average availability time, patch antenna

Alt ↓ | Beam →	90°	120°	160°
300 km	13.1 min	18.4 min	30.3 min
600 km	13.5 min	19.4 min	31.9 min
1000 km	14.6 min	21.1 min	34.1 min
2000 km	16.1 min	23.4 min	39.3 min
3000 km	17.1 min	26.7 min	44.1 min

Table 6: Average availability time, helix antenna

Alt ↓ | Beam ang →	180°	260°
300 km	9.9 min	29.7 min
600 km	10.3 min	31.3 min
1000 km	11.0 min	33.5 min
2000 km	12.0 min	38.8 min
3000 km	12.3 min	43.7 min

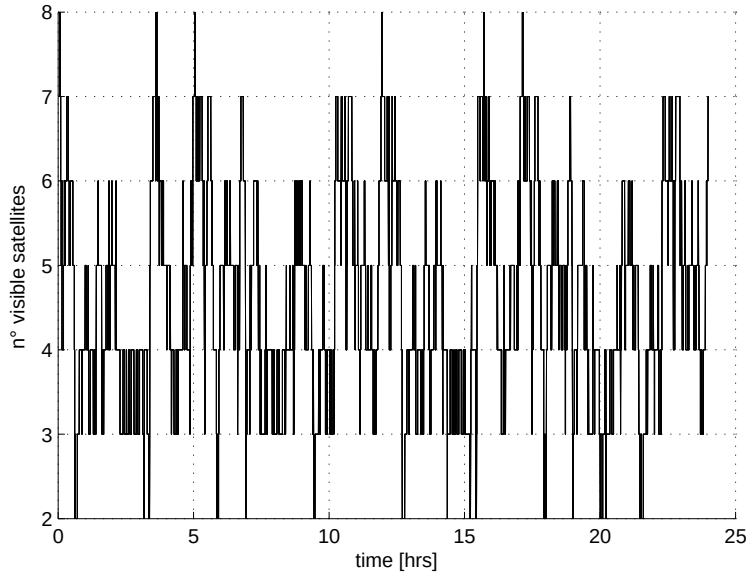

Figure 27: Number of visible satellites, patch antenna, bw=120°, alt=300km, i=0°

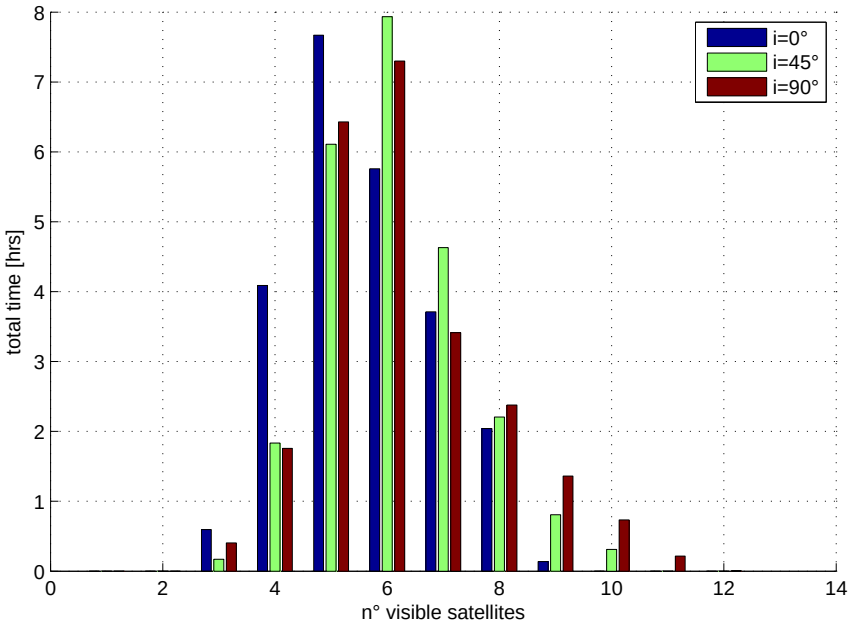

Figure 28: Cumulative number of visible satellites with different inclinations, patch antenna, bw=160°, alt=300km

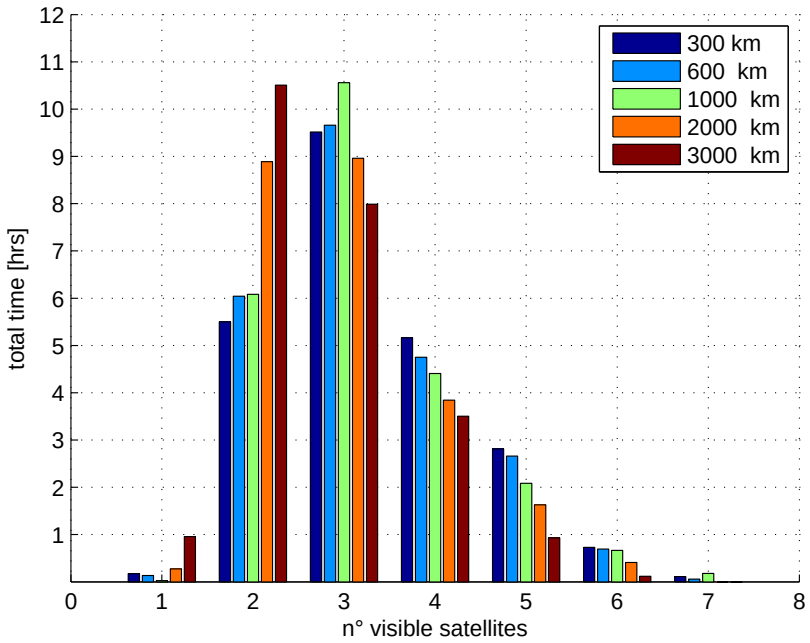

Figure 29: Cumulative number of visible satellites, patch antenna, bw=90°, i=0°

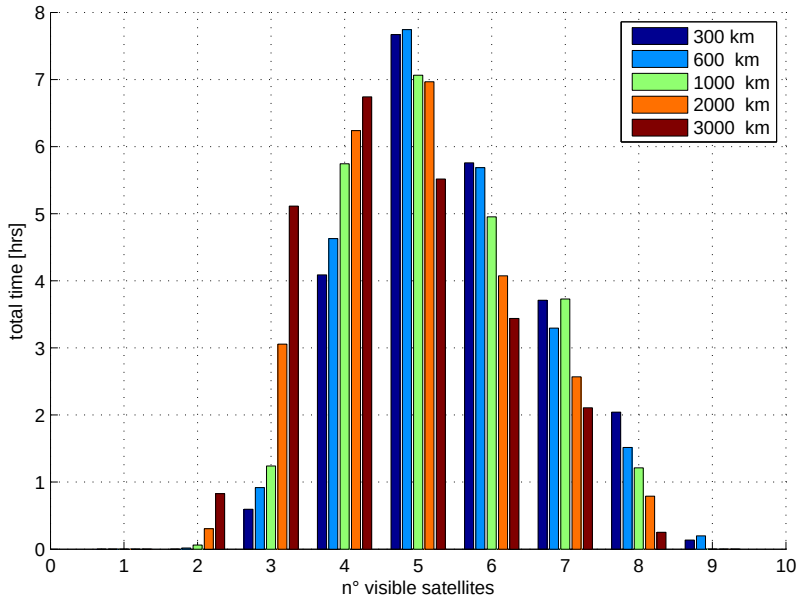

Figure 30: Cumulative number of visible satellites, patch antenna, bw=120°, i=0°

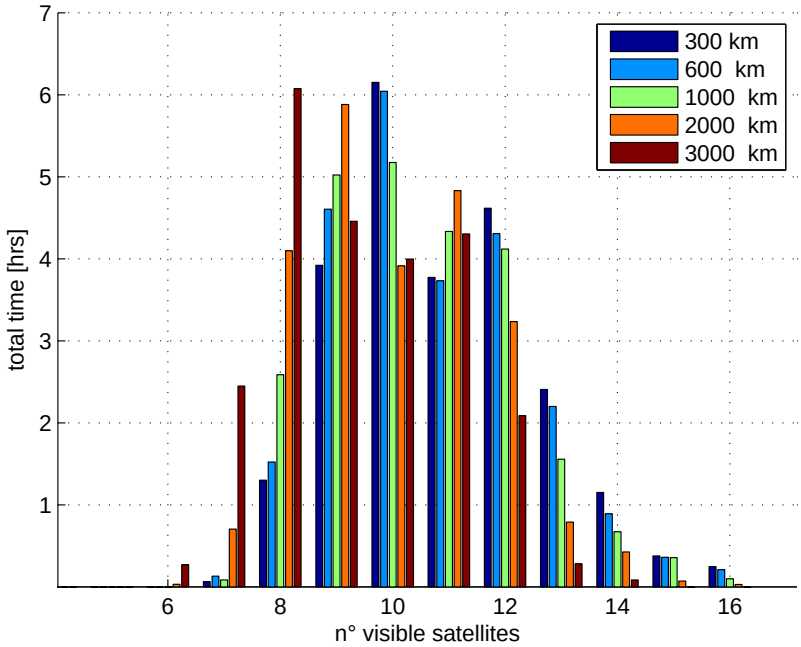

Figure 31: Cumulative number of visible satellites, patch antenna, bw=160°, i=0°

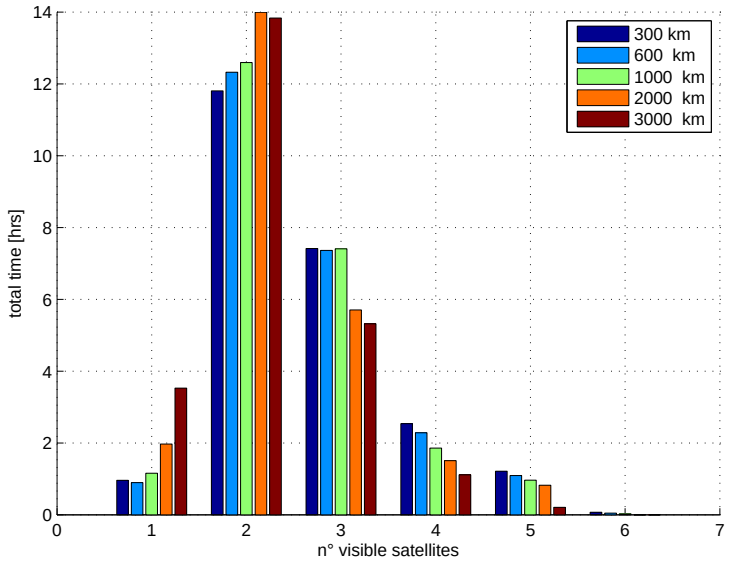

Figure 32: Cumulative number of visible satellites, helix antenna, bw=180°, i=0°

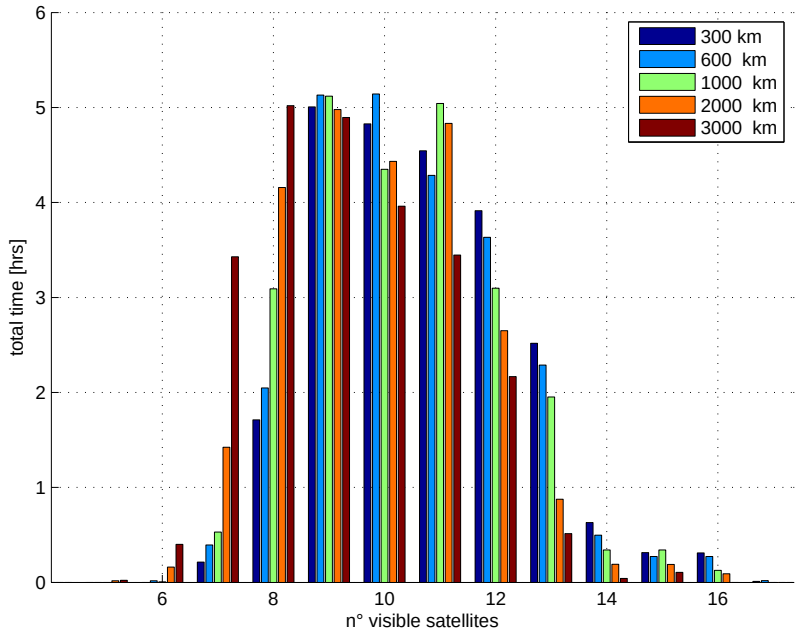

Figure 33: Cumulative number of visible satellites, helix antenna, bw=260°, i=0°

5 ATTITUDE ESTIMATION ACCURACY

SUMMARY

After having addressed the signal availability problem in the previous chapter the attitude estimation accuracy of the proposed system will be analysed.

The main error sources will be described and the ones most relevant to the problem modeled in the simulation software. After that the description of the simulation and an outline of its results will follow.

5.1 ERROR SOURCES

The first step in accuracy estimation is to identify, quantify and model the main error sources in the signal processing. The analysis follows Cohen[3] and takes advantage of some peculiarities of the differential GPS technique in order to neglect some of them. The error sources are:

- propagation
- multipath
- carrier to noise ratio
- antenna phase center
- receiver

Before detailing all these it is important to stress that the baseline length has a great influence in the errors propagation. If the cumulative error from all the sources is represented as a circle around the geometric location of the antenna this effect is clear: a shorter baseline implies a greater error, as shown in figure 34.

This effect is not avoidable and the only way to mitigate it is to try and minimize the cumulative error, that equals to reduce the diameter of the error circle.

Since the focus of this thesis is miniaturized satellites, with baselines around 10cm, the effects of these error are more relevant than in application with longer baselines.

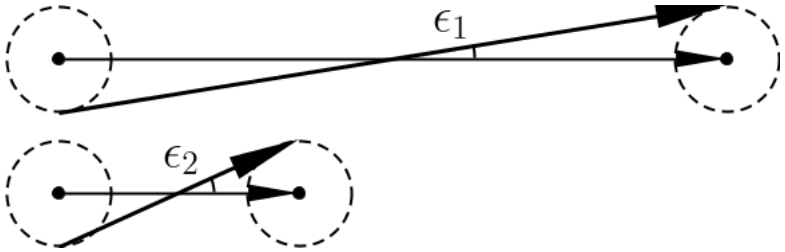

Figure 34: Effect of baseline length on baseline vector estimation in presence of errors

5.1.1 *Propagation*

Due to the fact that the GPS signals propagate through the atmosphere and the ionosphere they are subject to the Snell's Law and then follow a curved path rather than the expected straight-line one.

Since in the analysed application the antenna is at altitude of at least 300km these effects are not a great factor and they are not modelled.

Furthermore the very short baseline makes the signal arriving to the different antennas travel virtually the same path, so the disturbances are equal and they cancel themselves in differential measures.

5.1.2 *Multipath*

Multipath error comes from the multiple reflections of the incoming GPS signal on surfaces around the antenna, these reflected signals have different paths than the original signal and thus the carrier phase measured from them is different from the one on the original signal. This introduces error and a method is to be defined in order to discriminate the original signal from the reflections.

The fist way to reduce multipath is to place the antenna in such a way that it has clear field of view of the sky, however this is not always possible and in a complex structure such a spacecraft there can be a number of protruding elements, such communication antennas, gravity stabilization booms and solar panels, that can provide a reflecting surface for the signal.

One advantage of the Cubesat is that it has a very simple and compact design, usually the solar panels are not deployable and therefore there aren't structures that can cause multipath. The only remaining multipath effect can arise with low-incidence signals because the antennas are protruding from the panel, this can be addressed with the following considerations.

Since the GPS signal is polarized (right hand circular polarization, or RHCP) a reflection introduce a 180-degree shift in the polarization:

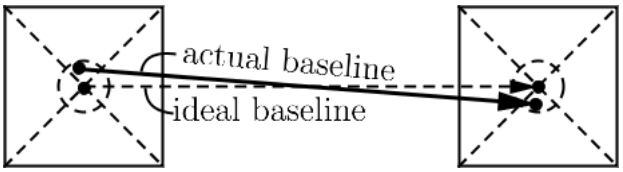

Figure 35: Effect of antenna phase center uncertainty on baseline definition

by making use of a polarized antenna, i.e. an antenna that is able to receive only right- or left-handed polarized signal, it is possible to ignore the noise coming from first reflection.

Moreover each reflection implies a decrease of the signal's power, so the original signal is always the one with the highest power: this is useful for discriminating the correct signal[24].

Multipath noise is not easily quantifiable due to its nature: it heavily depends on layout geometry and radiation pattern of the antenna group. Cohen [3] states that a differential range error of 5mm RMS models conservatively multipath for a typical application, this can be reduced by an order of magnitude by calibration of the antenna layout.

5.1.3 *Carrier to noise ratio*

This is the main source of error and it's closely related with the precision of the carrier phase tracking loop. Basically the higher this value (the higher the strength of the information with respect to the background noise) the easier will be for the receiver to track accurately the carrier phase. This accuracy is modeled as a random noise (uniform distribution) in the carrier phase measure, expressed either in mm or in deg; Lu [25] identified a value of 1mm RMS as a requirement for a DGPS attitude determination receiver.

5.1.4 *Antenna phase center*

This error is caused by the geometric extension of the antenna. In both in the simulation and the real attitude determination estimation the phase measurement refers to the geometric phase center of the antenna; the phase center in the actual antenna layout is not going to be in the center of the antenna neither its position is going to be stable, as it is usually function of the incidence angle of the signal. Figure 35 illustrates the problem for two patch antennas.

The uncertainty related to this phenomenon is modeled again as a random noise in the carrier phase measurement. In [26] the error is estimated around 1mm RMS, however it is possible to calibrate this

error for a single antenna by generating a lookup table of the phase center shift as a function of the incidence angle[7].

5.1.5 *Receiver specific error*

Within this denomination are grouped a number of phenomena that take place inside the receiving equipment or are related with it. This includes:

- Cross-talk: the electromagnetic interferences can be influential because of the several high gain stages, the effects of noise in the early stages can be increased exponentially; this can be controlled with proper design of the receiver and is not modelled.
- Line bias: since the electrical informations move at a constant speed, i.e. the speed of light in their medium, the phase of each antenna is delayed by a time proportional to the length of the cable from the antenna to the receiver; this is a systematic error and can be calibrated before use (this remains a factor if the cable is exposed to wide thermal cycles that can alter significantly its length).
- Local oscillator bias: this error is due to the use of different clocks inside the receiver (e.g. one for each channel, each channel can track the signal from one satellite), since the phase measure must be taken at exactly the same time for every channel the time difference from non synced clocks translates directly in false phase difference. By making use of a single clock and multiplexing the channels[3] this error is canceled.
- Inter-channel bias: this is similar to line bias but it is caused by different paths for each channel, using a multiplexed architecture this is again canceled.

While these errors are not modeled in the simulation they gave some insight in the inner working of the GPS receiver and on the many calibrations that needs to be carried out on the system, as well as the techniques that are used to reduce the error's impact.

Table 7: Modeled error sources and average values

Error source	Average value
Multipath	$0.5 \div 5mm$
C/No	$1mm$
Phase center	$1mm$

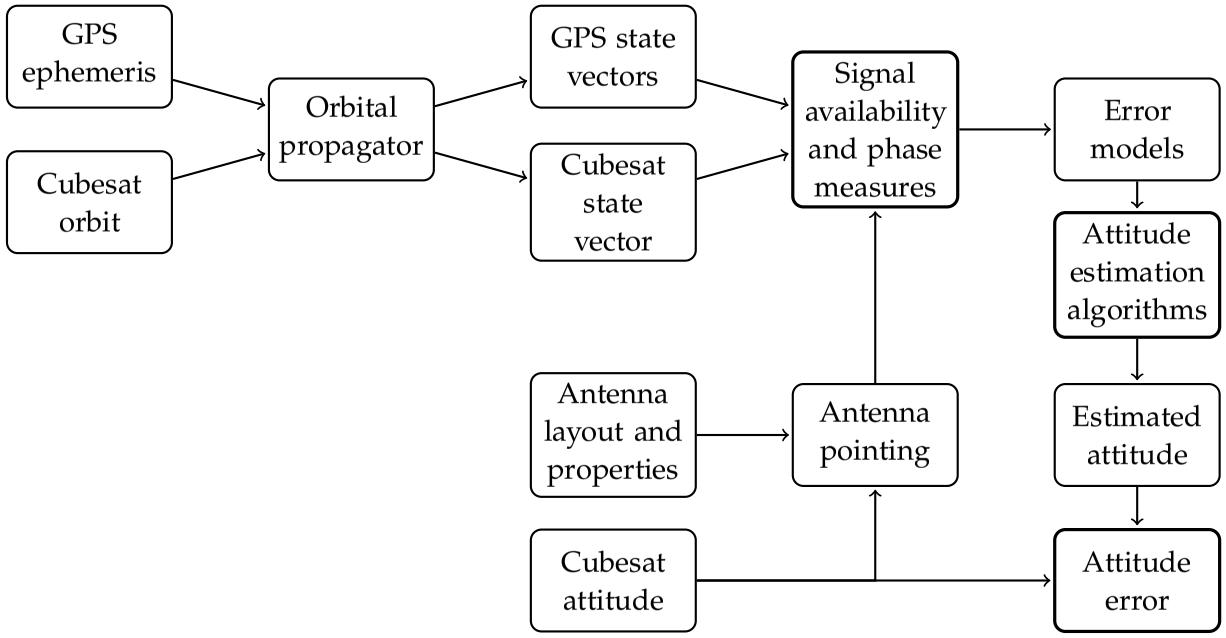

Figure 36: Block diagram of attitude estimation simulations

The simulation structure is similar to the one used in the previous analysis but with the addition of the attitude estimation procedure.

Table 7 sums up the results of the previous paragraphs and is the base for the error input in simulations. The single effects are combined in a single value, this perturbs the exact phase difference measure.

5.2.1 *Simulation procedure*

The basic configurations analysed are the same than the previous chapter, but some are discarded according to the visibility simulations results. For each case three error magnitude are analysed, representing a typical, best or worst case scenario.

- The *typical case* (2.5mm RMS) is obtained from table 7 and is representative of the performances of current available hardware with thorough calibration.
- The *best case* (1mm RMS) has been chosen arbitrarily in order to provide a perspective of the potentiality of next generation hardware.
- The *worst case* (7mm RMS) is again taken from table 7 but with poor or no calibration.

These RMS values are used to generate an uniform distribution interval with amplitude $a = \text{RMS}2\sqrt{3}$, this is used as the phase noise interval in the simulations.

The antenna layout considered are 120° and 160° for patch and 260° for helix, having discarded the 90° patch and the 180° helix; the altitude is ranging from 300 to 3000 km.

Figure 36 shows the structure of the simulation procedure in a block diagram. In particular the attitude determination algorithm follows closely the one presented in chapter 3 and has two steps:

- conversion from phase differences to vectorized measures
- application of the QUEST algorithm to estimate the attitude quaternion from the vectorized measures

The output of the QUEST algorithm is then converted from quaternions to Yaw-Pitch-Roll angles.

For each step of the simulation a statistical analysis has been performed in order to obtain the attitude error given the phase difference

errors, with a uniform distribution random noise and 1000 runs for every iteration. This allows to calculate the 3σ attitude error (3 times the RMS attitude error).

Two kinds of simulation has been carried out with different purposes:

- a short-timespan analysis that aims to evaluate the performances of the algorithm as a real-time attitude estimator. The time step is 1 second, equivalent of the frequency of a typical embedded GPS receiver (the time required to process the signal and perform attitude estimation), for a total time of 2 hours.
- a longer analysis in order to characterize the overall accuracy of the system, for a total time of 24 hours and a time step of 10 seconds.

5.2.2 *Simulation results*

5.2.2.1 *Patch*

The first plot (figure 38) represent the attitude estimation results for the three attitude angles for one of the analysed cases. The yaw, pitch and roll angles error are obtained by subtracting the estimated values from the nominal values; also the number of available GPS satellites and the 3σ bounds for the attitude estimation are given.

On this figure several considerations can arise:

- It is clear that when the number of available measures (n) is less than 3 the attitude algorithm can't provide an attitude estimation, such as in the period between 0.6 and 0.8 hour
- The attitude estimation accuracy is strongly dependent on n: when $n = 3$ the 3σ bound is as high as $5°$, while for $n = 8$ the same is less than $1°$
- The direction of the sightline versors is also influential: around 1.4 and 1.6 hours the 3σ bound for the roll and yaw angles is much higher than the one for the pitch error.

From a similar figure another aspect that characterize the DGPS attitude estimation is evident: the yaw accuracy is generally better than the pitch and roll accuracy.

This is a consequence of the QUEST algorithm, if more signals (and thus baselines) are available from satellite low on the horizon the estimation of the yaw angle is better (the yaw axis is parallel to the zenith axis), on the contrary if the satellites are concentrated around the zenith the pitch and roll estimation is favoured; this is shown in figure 37.

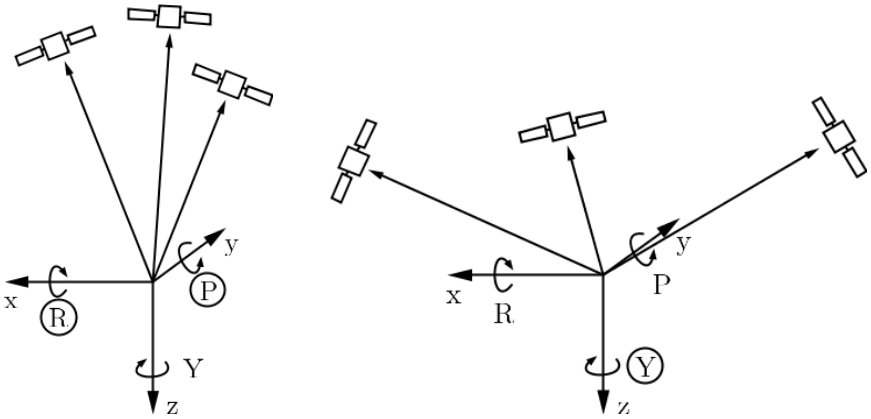

(a) Best for roll and pitch (b) Best for yaw

Figure 37: Influence of sightline geometry on attitude accuracy

This result is consistent with the attitude accuracy estimation of the RADCAL satellite, performed in [4] and outlined briefly in table 2.

Comparing figures 38 and 39 it can be noted that, while the accuracy difference varies greatly when passing from 3 to 4 visible satellites, the visibility of more than 10 doesn't offer the same advantage.

Figures 40 and 41 present the results for the patch antenna layout with two different bandwidth, respectively 120° and 160°. The bw=120° at an altitude h=3000km has not been considered because of the very low number of GPS satellites available.

5.2.2.2 *Helix*

The only case considered for the helix antenna layout is the bw=260°, the other one (180°) having too few available satellites as shown in the previous analysis in chapter 4.

The results are very similar with the best case patch antenna bandwidth (figure 42), this is consistent with the visibility analysis that leads to the same conclusion than the one in the previous chapter: the helix antenna layout doesn't offer substantial advantages with respect to the patch antenna layout.

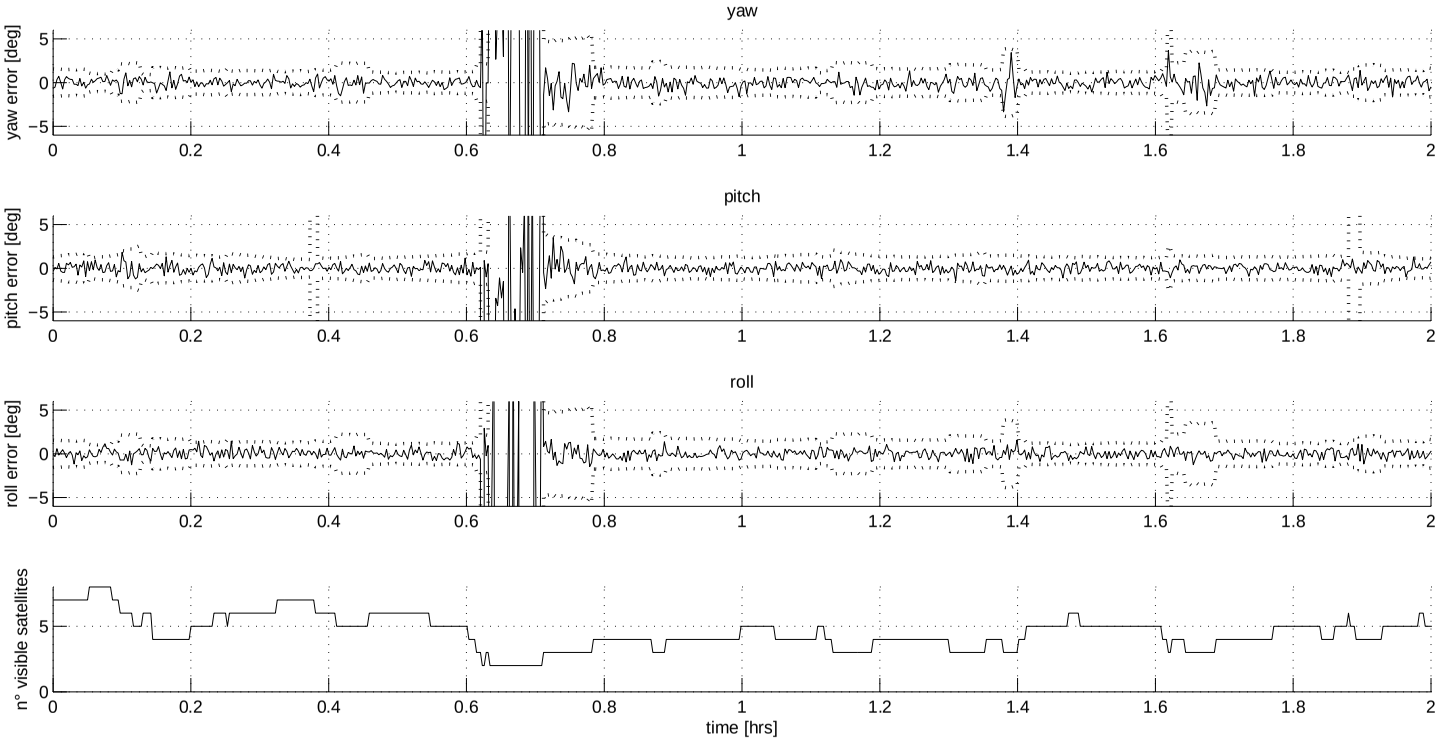

Figure 38: Attitude estimation accuracy, patch antenna, bw=120°, h=300km, noise=2.5mm. The dotted lines are the 3σ bound for attitude error

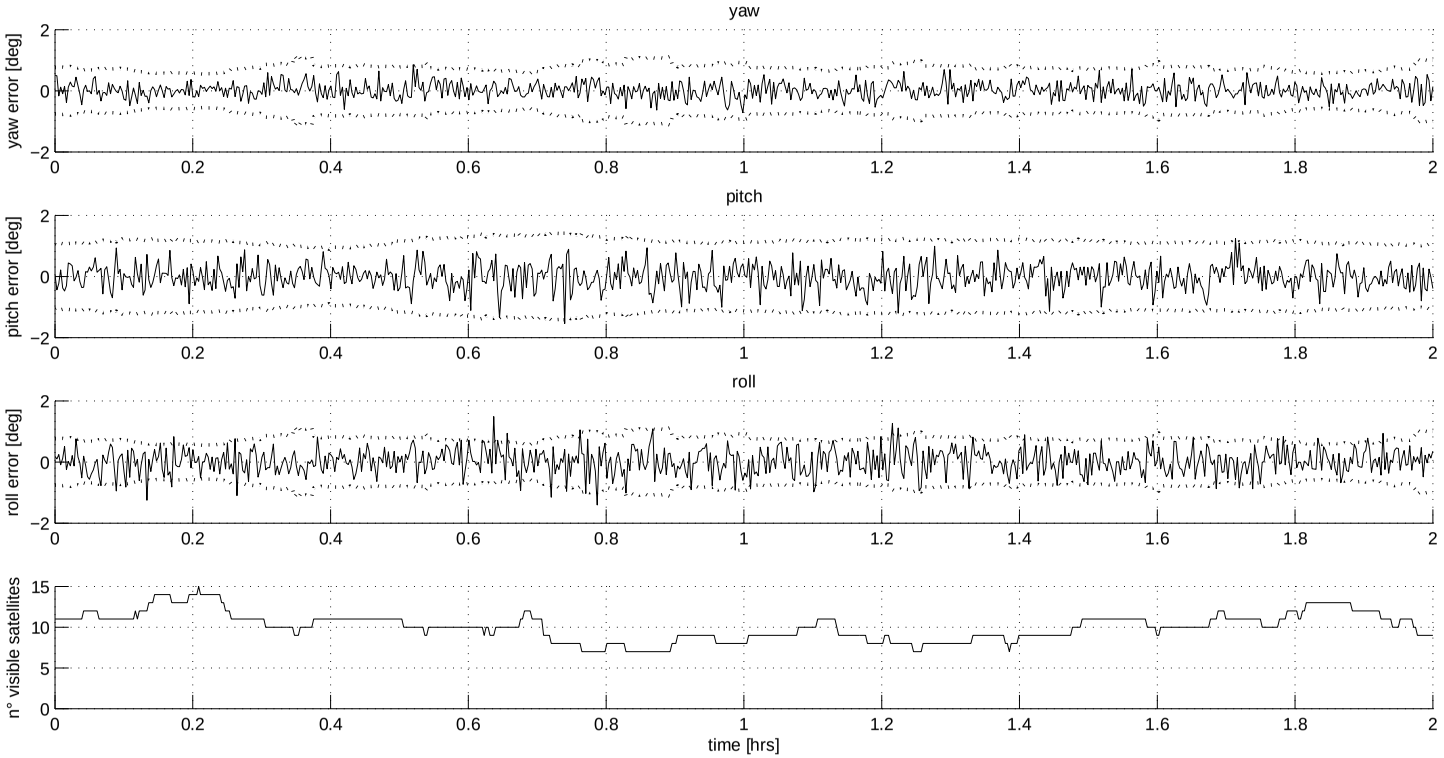

Figure 39: Attitude estimation accuracy, patch antenna, bw=160°, h=300km, noise=2.5mm. The dotted lines are the 3σ bound for attitude error

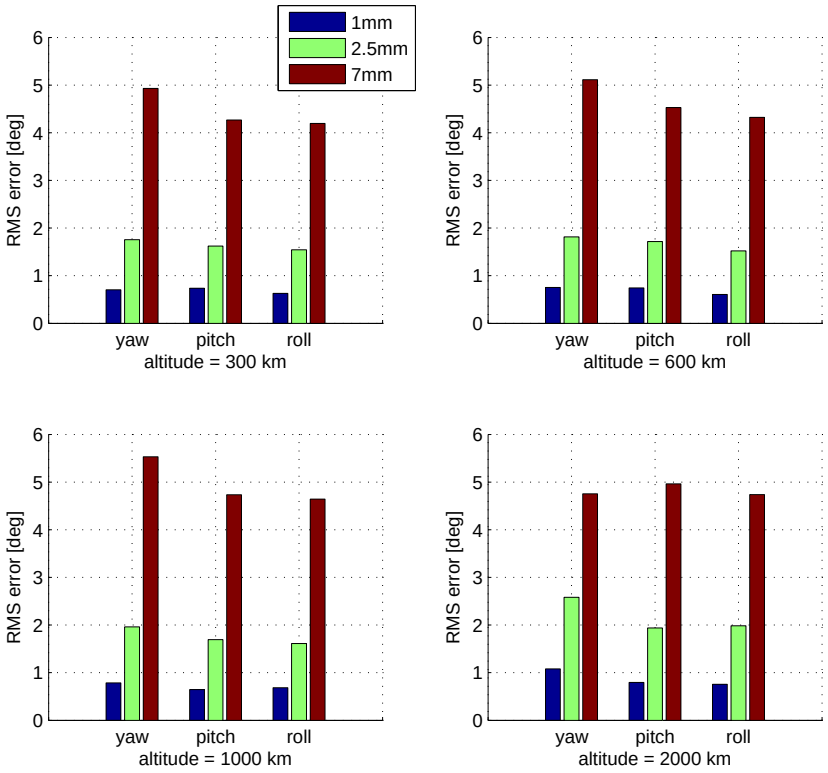

Figure 40: Average 3σ attitude error, patch antenna, bw=120°

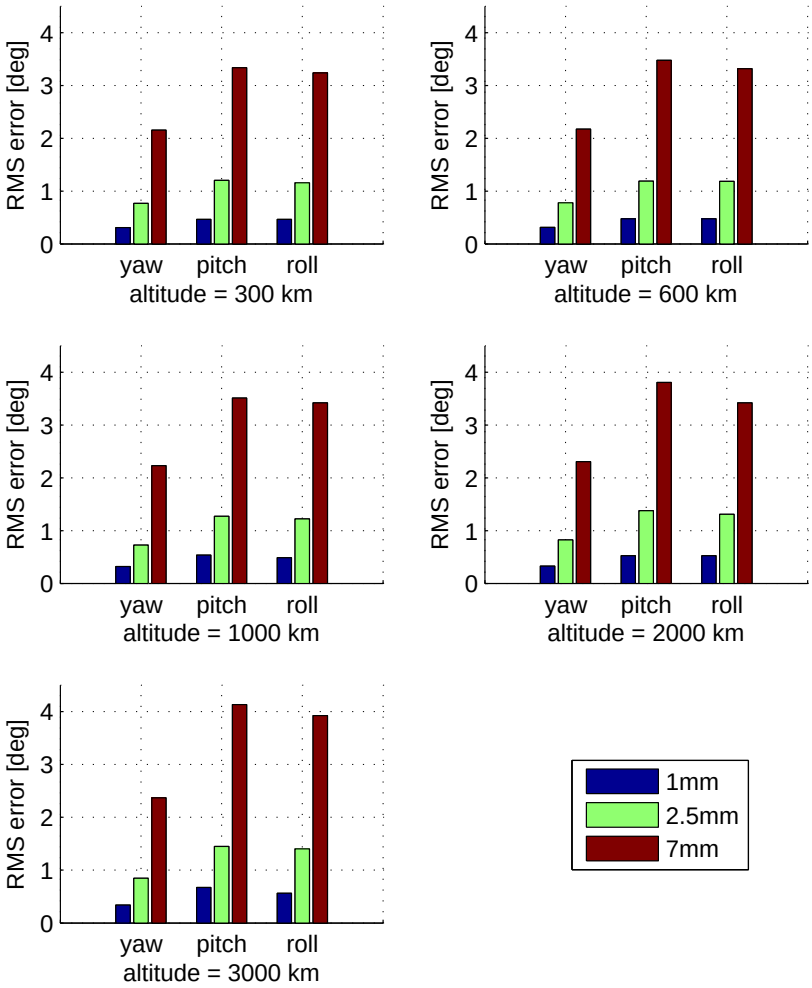

Figure 41: Average 3σ attitude error, patch antenna, bw=160°

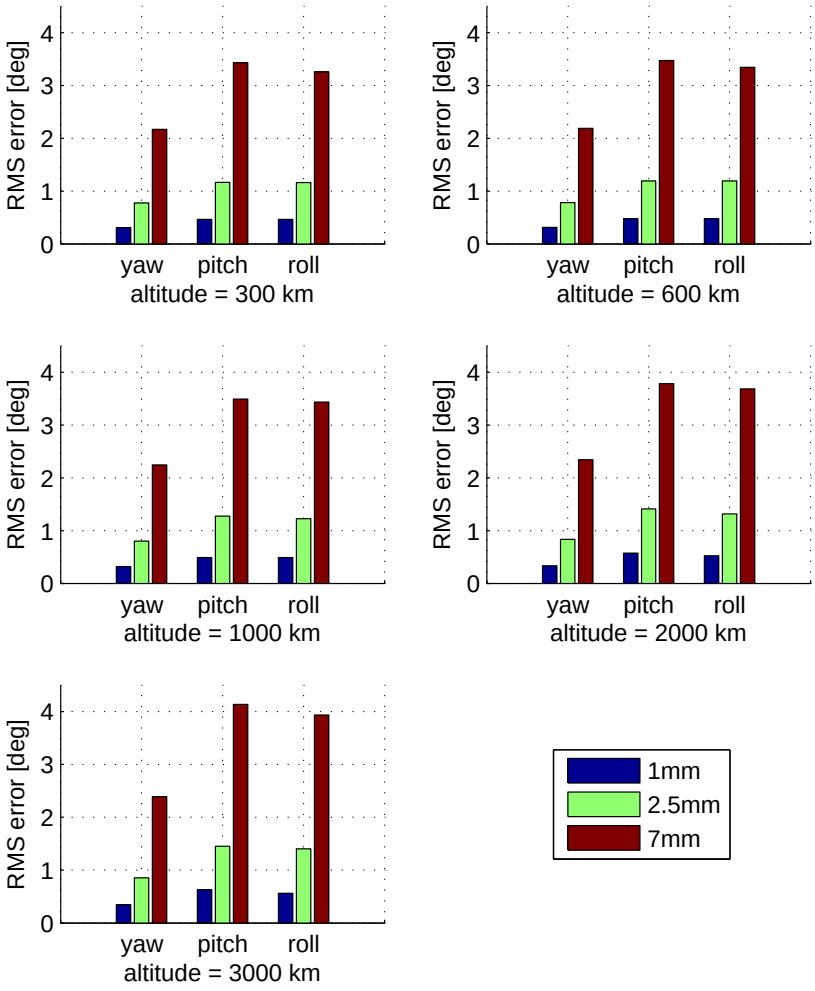

Figure 42: Average 3σ attitude error, helix antenna, bw=260°

6 CONCLUSIONS

6.1 DESIGN EVALUATION

Of the two proposed layouts the one exploiting patch antennas is deemed the better, for several reasons:

- simpler mechanical design and better compatibility with the Cubesat standard
- lower geometric envelope of the patch antennas with respect to helix antennas
- comparable performances with the helix antenna layout in terms of attitude accuracy

However this design is not free from disadvantages:

- higher multipath effect
- higher influence of antenna positioning and ground plane (the panel on which the antennas are mounted) in the radiation pattern

The former can be solved by making use of polarized patch antennas, while the latter can be evaluated only with hardware tests.

Summing up the results of the analysis performed through the previous chapters it is possible to compare the proposed design with the RADCAL and TOPSAT experiments, with the caveat that the TOPSAT results are actually the discrepancy of the DGPS attitude solution with the primary ADCS attitude solution; this is shown in table 8.

The comparison of the RADCAL and the second Cubesat, with similar phase noise, allows to appreciate the influence of the baseline length on the attitude accuracy: the error is more than doubled when passing from 0.6m to 0.1m.

This shifts the focus on optimization of the receiving hardware in order to minimize the errors that affect the phase difference measures, the 1 and 2.5 mm phase noise cases can give a good example of the performances to be expected with the improvement of the receivers.

The implementation of FPGA technologies is another factor that can contribute to the effectiveness of the system, lowering the average time-to-lock and granting more flexibility in the receiver's design.

Table 8: Comparison of 3σ attitude errors for RADCAL, TOPSAT and the proposed DGPS sensor

	RADCAL	TOPSAT	Cubesat	Cubesat	Cubesat
Phase noise	8mm	NA	7mm	2.5mm	1mm
Yaw	0.951°	1.5°	2.245°	0.788°	0.321°
Pitch	1.485°	1.83°	3.652°	1.297°	0.534°
Roll	1.488°	2.13°	3.514°	1.255°	0.506°

6.2 COMPARISON WITH AVAILABLE MINIATURE SATELLITE ADCS

The recent growth in Cubesat mission numbers is accompanied by an increasing number of commercial off-the-shelf attitude determination sensors and systems available for purchase[1].

The most common sensors include magnetometers, Earth and Sun sensors; however even star trackers have been recently developed for Cubesat applications that have more stringent attitude control requirements.

Usually Earth and Sun trackers are the least accurate, they can provide only two reference vector and this, combined with the inherent limits of the sun and nadir vector knowledge (see table 1), limits their overall accuracy. As an example *MAI-SES Static Earth Sensor*[2] has an attitude accuracy 1.5° at 3σ, magnetometers have similar performances.

Star trackers offers higher performances: the *ST-200 Star Tracker*[3] has a pitch/yaw accuracy (rotation perpendicular to its focal axis) of 30 arcsec (0.025° @ 3σ) and a roll accuracy (rotation around its focal axis) of 400 arcsec (0.3° @ 3σ).

Within this context the DGPS attitude sensor can be a competitor with the Earth and Sun trackers for 3-axis stabilized spacecraft, with the advantages that the attitude estimation independent from the orbit position (no eclipses) and the system can provide also an accurate orbit position estimation with standard GPS features.

A complete ADCS suite that make use of DGPS attitude estimation may be composed of:

1 An exhaustive list of suppliers of Cubesat components is available at http://www.cubesat.org/index.php/collaborate/suppliers

2 Data retrieved from http://www.cubesatshop.com

3 Data retrieved from http://http://www.berlin-space-tech.com

- four patch antennas and a FPGA-based receiver to provide DGPS attitude estimation
- three magnetometers and three magnetotorquers as a detumbling system: after its release the spacecraft is likely to be in a tumbling (rapidly and randomly rotating) motion and external torques are required to stabilize the attitude.
- a miniaturized IMU with MEMS technology: this are required in the event of temporary loss of lock of the DGPS system and also to provide a precise angular velocity measure if needed[4].

6.3 FUTURE WORK

Several areas of future work have been identified throughout the course of the thesis:

6.3.1 *In-depth receiver simulation*

In order to have a detailed analysis of the satellite availability and accurate prediction of the carrier to noise error the simulation of the complete GPS receiver is required. This allows the calculation a more representative value of the overall phase noise error.

6.3.2 *Kalman filtering*

The Kalman filter is an algorithm that combines a series of measurements over time and a model of the system's behaviour in order to obtain a more accurate estimate of the observed quantities.

This algorithms has been developed specifically for Guidance, Navigation and Control (GNC) applications and its usage is very common in attitude determination software [2].

It is believed that by making use of the Kalman filter the attitude estimation accuracy will further improve.

6.3.3 *Experimental test*

The predicted performance of the DGPS system are overall very promising, however even a deeper numerical analysis can't provide accurate result without a test of the antenna layout, with particular regard to radiation pattern modeling.

For this reason the realization of an experimental testbed is suggested.

4 The TOPSAT mission previously described makes use of an image enhancement technology that requires the same area to be observed more than once, this imposes a very precise knowledge of attitude rates but a more relaxed requirement for attitude itself

BIBLIOGRAPHY

[1] F. Landis Markley and Daniele Mortari. Quaternion attitude estimation using vector observation. *The Journal of the Astronautical Sciences*, 48(2):359–380, April-September 2000.

[2] James R. Wertz. *Spacecraft Attitude Determination And Control*. Kluwer Academic Publisher, 1978.

[3] Clark Emerson Cohen. Attitude determination using gps. Master's thesis, Stanford University, 1992.

[4] John C. Stoll. Performance analysis of a gps interferometric attitude determination system for a gravity gradient stabilized spacecraft. Master's thesis, Massachussets Institute of Technology, 1995.

[5] E. G. Lightsey. *Development and Flight Demonstration of a GPS Receiver for Space*. PhD thesis, Stanford University, 1995.

[6] M. ; Hebden R. ; Hodgart M.S. Duncan, S. ; Unwin. In-orbit demonstration of a gps attitude sensor. In *Satellite Navigation Technologies and European Workshop on GNSS Signals and Signal Processing (NAVITEC), 2010 5th ESA Workshop on*, 2010.

[7] Bageshwar et al. Minnesat: Gps attitude determination experiments onboard a nanosatellite. In *20th Annual AIAA/USU Conference on Small Satellites*, 2006.

[8] P. Axelrad B. Parkinson, J. Spilker Jr. and P. Enge. *Global Positioning System Theory and Applications*. American Institute of Aeronautics and Astronautic, Inc., 1996.

[9] Lawrence R. Weill Mohninder S. Grewal and Angus P. Andrews. *Global Positioning Systems, Inertial Navigation, and Integration*. Wiley, 2007.

[10] M. D. Shuster and S. D. Oh. Three-axis attitude determination from vector observation. *Journal of Guidance and Control*, 4(1):70, January-February 1981.

[11] Grace Wahba. Problem 65-1: A least squares estimate of satellite attitude. *SIAM Review*, 7(3):409, 1965.

[12] Paul B. Davenport. A vector approach to the algebra of rotations with applications. Technical report, NASA Goddard Space Flight Center, 1968.

[13] F. Landis Markley. Atttitude determination using vector observation and the singular value decomposition. *The Journal of the Astronautical Sciences*, 38(3):245–258, July-September 1988.

[14] F. Landis Markley. Atttitude determination using vector observation: A fast optimal matrix algorithm. *The Journal of the Astronautical Sciences*, 41(2):261–280, April-June 1993.

[15] Daniele Mortari. Esoq: A closed-form solution to the whaba problem. In *Sixth Annual AIAA/AAS Space Flight Mechanics Meeting*, Austin, TX, Feb. 11-15 1996.

[16] Daniele Mortari. Esoq-2 single-point algorithm for fast optimal spacecraft attitude determination. In *7th Annual AIAA/AAS Space Flight Mechanics Meeting*, Huntsville, AL, Feb. 10-12 1997.

[17] John Crassidis Landis and F. Landis Markley. A new algorithm for attitude determination using global positioning system signals. *AIAA Journal of Guidance, Control, and Dynamics*, 20:891–896, 1997.

[18] Constantine A. Balanis. *Antenna theory analysis and design*. Wiley, 1997.

[19] James Bao-Yen Tsui. *Fundamentals of GPS Receivers*. Wiley, 2000.

[20] Charles H. Frey Jennifer L. Ruiz. Geosynchronous satellite use of gps. In *ION GNSS 18th International Technical Meeting of the Satellite Division*, Long Beach, CA, 13-16 September 2005.

[21] *GPS Antennas, RF Design Considerations for u-blox GPS Receivers*. retrieved 29/09/2014 from www.u-blox.com.

[22] A. ; Motawie I. Hamza, G. ; Zekry. Implementation of a complete gps receiver using simulink. *Circuits and Systems Magazine, IEEE*, 9(4):43–51, Fourth Quarter 2009 2009.

[23] Alex Aaen Birklykke. High dynamic gps signal acquistion. Master's thesis, Aalborg University, 2010.

[24] C.J. ; Macdoran P.F. Axelrad, P.; Comp. Snr-based multipath error correction for gps differential phase. *Aerospace and Electronic Systems, IEEE Transactions on*, 32(2):650 – 660, April 1996.

[25] Gang Lu. *Development of a GPS Multi-Antenna System for Attitude Determination*. PhD thesis, University of Calgary, 1995.

[26] Jose L. Padilla Gonzalo Exposito-Dominguez Manuel Sierra-Castaner Pablo Padilla, Jose M. Fernandez and Belen Galocha. Comparison of different methods for the experimental antenna phase center determination usign a planar acquisition system. *Progress In Electromagnetics Research,*, 135:331–346, 2013.